Wake asymmetry of yaw state wind turbines induced by interference with wind towers

Shibuya, Koichiro
Major of Mechanical and Systems Engineering, Interdisciplinary Graduate School of Engineering Sciences, Kyushu University

Uchida, Takanori
Research Institute for Applied Mechanics (RIAM), Kyushu University

出版情報：Energy. 280, pp.128091-, 2023-10-01. Elsevier
バージョン：

Energy 280 (2023) 128091

Contents lists available at ScienceDirect

Energy

journal homepage: www.elsevier.com/locate/energy

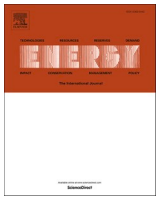

Wake asymmetry of yaw state wind turbines induced by interference with wind towers

Koichiro Shibuya [a,*], Takanori Uchida [b]

[a] Major of Mechanical and Systems Engineering, Interdisciplinary Graduate School of Engineering Sciences, Kyushu University, 6-1 Kasuga-koen, Kasuga, Fukuoka, 816-8580, Japan
[b] Research Institute for Applied Mechanics (RIAM), Kyushu University, 6-1 Kasuga-koen, Kasuga, Fukuoka, 816-8580, Japan

ARTICLE INFO

Handling Editor: Jesse L. The

Keywords:
Wind turbine wakes
Wake control
Yaw steering
Bluff body
Wind farm

ABSTRACT

Wind turbine wakes are known to cause significant reductions in power generation and increased load on downwind wind turbines. Therefore, controlling wind turbine wakes is crucial, and yaw steering is considered one of the most effective methods of doing so. In this study, wind tunnel experiments using a wind turbine model and Large-eddy simulations (LES) were conducted to gain a better understanding of the wake of a yawed wind turbine. The results showed a clear difference in the horizontal distribution of wake velocity at hub height for positive and negative yaw angles, as well as both lateral and vertical wake deflections. Further investigation revealed that wind towers have a significant effect on the wakes of yawing wind turbines. For positive yaw angles, the velocity deficit is larger above the rotor, resulting in a vertical wake shape caused by the interference between the blade wakes and detached flow from the tower. Conversely, for negative yaw angles, the velocity deficit is larger below the rotor, resulting in a horizontal wake shape. These findings will facilitate the development of more accurate wake models and control methods.

1. Introduction

Clean energy is being promoted due to concerns about abnormal weather associated with global warming. In particular, wind power generation is shifting from onshore to offshore, where the energy density is higher, and further development is expected. In recent years, wind farms have become popular, with multiple wind turbines installed in the same location to efficiently generate large amounts of power while reducing construction and maintenance costs. Additionally, when wind turbines are installed offshore, they are arranged more densely to shorten the distance between turbines and reduce the cost of the transmission line. However, when a wind turbine operates, wakes form behind the wind turbine, which has a negative impact on other wind turbines.

Fig. 1 shows a schematic illustration of a wind turbine wake [1]. The kinetic energy of the wind entering the wind turbine is converted to rotational energy of the blades, resulting in a decrease in wind speed during interference by the wake. In addition, a highly turbulent flow field is formed in the wake due to the complex interference of swirling currents caused by the rotation of the wind turbine blades and vortexes ejected from the blade tips or detached from the hub and tower. If another wind turbine located downwind operates in response to a wake with reduced wind speed, not only will the wind turbine generate less power, but it will also have a shorter lifespan due to turbulence. Thomsen and Sørensen [2] used measurements from the Vindeby wind farm and concluded that the increase in wind farm fatigue load due to the turbine wake is between 5% and 15%.

To keep the operating costs low and continue to generate large amounts of electricity, controlling wind turbine wakes to minimize their effects is necessary. Various methods have been proposed to control wind turbine wakes [3,4], including axial induction control (AIC), which suppresses wakes by controlling the pitch angle of wind turbine blades and generator torque; yaw steering, which deflects wakes by generating lateral drag on the wind turbine rotor through yaw misalignment; and a combination of these methods.

Yaw steering intentionally applies yaw misalignment to the wind turbine to deflect the wake. Although the wind turbine with an inclined wind-receiving surface generates less power, controlling the wake so that it does not hit the wind turbine on the downwind side is expected to increase the overall power generation of the wind farm. Numerical simulations by Ciri et al. [5] and wind tunnel experiments by Uchida et al. [6] confirmed that yaw steering deflects the wakes of wind turbines and increases the amount of power generated by downwind

* Corresponding author.
E-mail address: shibuya.k@hitachizosen.co.jp (K. Shibuya).

https://doi.org/10.1016/j.energy.2023.128091
Received 12 January 2023; Received in revised form 7 June 2023; Accepted 9 June 2023
Available online 12 June 2023

Nomenclature

x	Streamwise coordinate
y	Spanwise coordinate
z	Vertical coordinate
$\overline{u}$	Filtered instantaneous streamwise velocity
$\overline{v}$	Filtered instantaneous spanwise velocity
$\overline{w}$	Filtered instantaneous vertical velocity
$\overline{p}$	Filtered instantaneous dynamic pressure
Re	Reynolds number
f_i	External force
τ_{ij}	SGS stress (SGS: sub-grid scale)
ν_{SGS}	SGS eddy viscosity coefficient
$\overline{S}_{ij}$	Resolvable-scale strain rate tensor
k_{es}	Velocity scale squared
T_s	Time scale
C_{MTS}	Model parameter
Δ	Filter length scale

turbines. In a field study conducted by Bromm et al. [7] on a wind farm with a 3.5 MW wind turbine installed, it was confirmed that at a yaw angle of 20 deg, the wakes were deflected by a maximum of 0.2D (where D is the rotor diameter of the wind turbine).

As shown in various studies, yaw steering has a positive impact on wind farms. In recent years, many studies have been reported on optimizing wind farms using optimization algorithms and trial-and-error methods based on yaw-steering techniques [8–16]. Two main approaches have been used to represent wakes of yawing wind turbines in wind farm optimizations: Large-eddy simulations (LES) and analytical wake modeling. Since LES requires a significant amount of computational resources, it is preferable to use a wake model to optimize wind farms in a shorter time for commercial use. Constructing a highly accurate wake model is crucial, as multiple wind turbines generate wakes and interfere with each other in a wind farm. For instance, Qian and Ishihara [14] developed a wake model [17] that can simulate yaw steering while predicting both wind speed and turbulence intensity in the case of wake interference and applied it to wind farm optimization.

However, there are still many unclear points in relation to the wake during wake steering operations (hereinafter referred to as yaw state). LES analysis of wind farms by Archer and Vasel-Be-Hagh [8] and Fleming et al. [18] reported that even for the same magnitude of yaw misalignment, there is a difference in the output obtained at the downwind wind turbine when the direction of misalignment is different, as shown in Fig. 2. Fleming et al. [19] and Miao et al. [20] also conducted numerical simulations with different yaw misalignment directions and reported different wake vortex structures in opposite yaw conditions. These previous studies suggest that the wakes become asymmetric with respect to the flow direction depending on the direction of yaw angle. However, existing analytical wake models do not take this effect into account, as pointed out by Fleming et al. [19], and deflect the same amount for the same magnitude of yaw angle, resulting in axisymmetric wakes. For a more accurate prediction of the flow field in a wind farm, it is necessary to understand exactly what causes the wakes to be axisymmetric at opposite yaw angles.

In this study, we aim to investigate the mechanism behind the observed wake asymmetry during yaw steering operations. In addition to previous studies by Fleming et al. [19] and Miao et al. [20], we focused on the interference between the bluff body and wind turbine wakes. Previous research has pointed out the interference between wakes and hub vortices emitted from nacelles in wind turbines without wake steering [21–24], as well as the interference between wakes and tower detached flow in wind tunnel experiments, LES, and field studies [25–27]. Specifically, Pierella and Saetran [25] conducted wind tunnel experiments and reported that the vertical downward advection of wind turbine wakes under the influence of the tower causes left-right asymmetry in the wake vortex structure. In the yaw state, differences in the wake vortex structure in each yaw direction are assumed to be caused by the interference between the bluff body detached flow and the blade wakes.

This study conducted wind tunnel experiments using a wind turbine model to confirm the asymmetry of the yaw wake, and measured the flow in the near-wake region of the wind turbine. The experimental results were supplemented with LES to further investigate the interference between the bluff body and wakes.

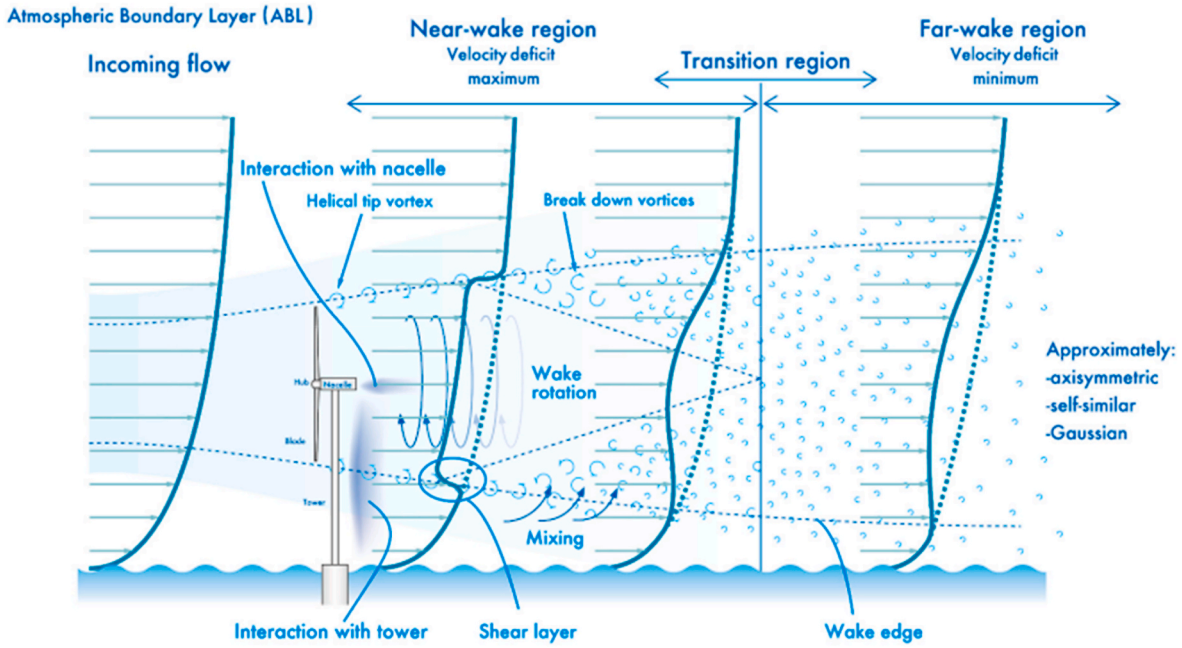

Fig. 1. Schematic side view of the wake structure behind a single wind turbine [1].

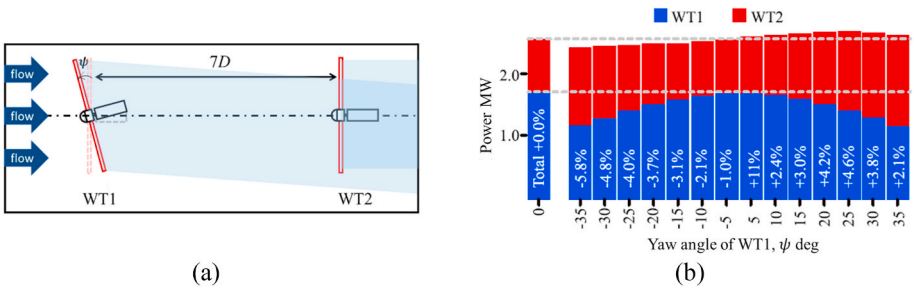

Fig. 2. The total power of two turbines varies with the yaw angle [18].

2. Methodology

2.1. Wind tunnel experiments

2.1.1. Wind tunnel and turbine model

Experiments were conducted using the circulating boundary layer wind tunnel depicted in Fig. 3 and the wind turbine model shown in Fig. 4. The test section of the wind tunnel was 15 m long, 3.8 m wide, and 2 m high, and the side walls and top plates of test section Nos. 3 to 5 were removed to minimize the blockage effect. The wind turbine model installed in the wind tunnel is detailed in Fig. 5, with a rotor diameter of $D = 0.442$ m and a hub height of 1 m. The model had a servomotor in the nacelle, which controlled the rotation of the aluminium MEL blades. "MEL" stands for the initials of Mechanical Engineering Laboratory, and the blades were developed by Matsumiya et al. [28]. Fig. 6 shows a cross-sectional view of the blade from the root to the tip, including the position of the center of gravity of each section. Fig. 7 shows the chord length and twist angle variations from the root to the tip of the blade, while Fig. 8 shows the lift coefficient C_L and drag coefficient C_D versus the angle of attack for the blade section located at 75% from the rotor center.

In this experiment, the MEL blade was rotated at a tip speed ratio of 4.25 (2755 rpm), which maximizes the power coefficient Cp of the MEL blade, at an inlet wind speed of $Uin = 15$ m/s. The flow field behind the wind turbine was measured under conditions of active wake formation in the wind turbine model. The Reynolds number for this experiment, calculated from the wind tunnel height and the rotor diameter of the wind turbine model, was $Re = 4.5 \times 10^5$.

2.1.2. Wake measurement methodology

To measure the wake velocity at the hub height behind the wind turbine model, an ultrasonic anemometer attached to a traverser was used, as shown in Fig. 9. The origin was set at the center of the rotor of the wind turbine model. The yaw angle ψ of the wind turbine model was defined as positive counter-clockwise when viewed from above and was rotated around the origin. The measurements were taken for a total of five yaw state patterns with ψ ranging from −30 deg to +30 deg in 15 deg increments. To obtain the horizontal distribution of the wakes, the traverser was moved 30 mm in the orthogonal direction to the mainstream at the end of each 30-s measurement. The sampling frequency for the measurements was 1 kHz, and the low-pass filter was set at 100 Hz. A second ultrasonic anemometer was installed upstream of the wind tunnel to control the wind velocity entering the wind tunnel. The voltage values obtained from the ultrasonic anemometer were converted to A/D, as shown in Fig. 10, and then fed into a PC.

To investigate the effect of the open and closed conditions of the wind tunnel, the horizontal wake distributions formed by the wind turbine model were compared for both conditions. Fig. 11 illustrates the dimensionless mean velocity (= u/Uin) horizontal distributions at hub heights of $x = 3D$ and $6D$ (where D is the rotor diameter) behind the wind turbine, with a fixed yaw angle of $\psi = +30$ deg. According to Sedaghatizadeh et al. [29], the velocity distribution of a wind turbine wake is affected by the presence or absence of a wall. It was determined that the presence or absence of the wind tunnel wall had an impact on the distribution, as depicted in Fig. 11. However, the difference was minor, and the wind tunnel wall had no effect on the region from the vicinity of the wind turbine to the rear at $x = 6D$ in this study.

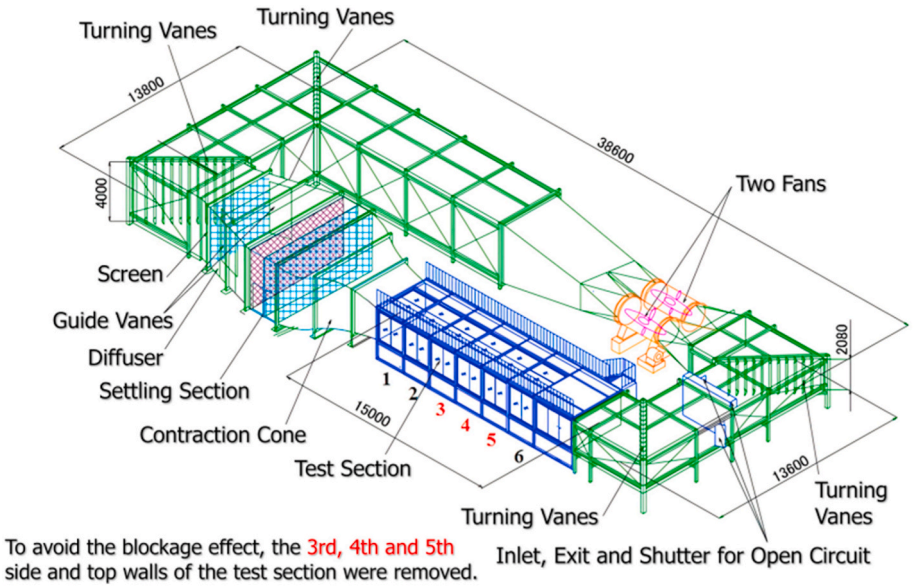

Fig. 3. Schematic diagram of the wind tunnel facility.

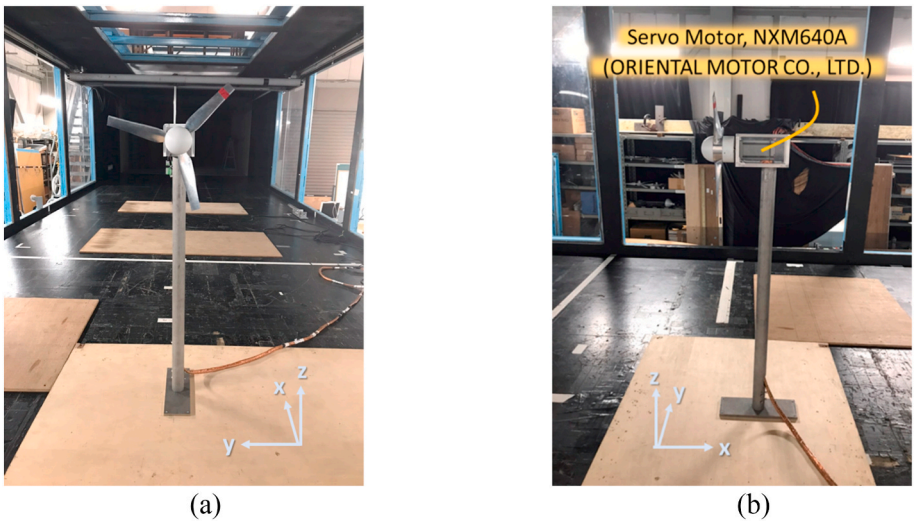

Fig. 4. Appearance of the wind turbine model: (a) front view, (b) side view.

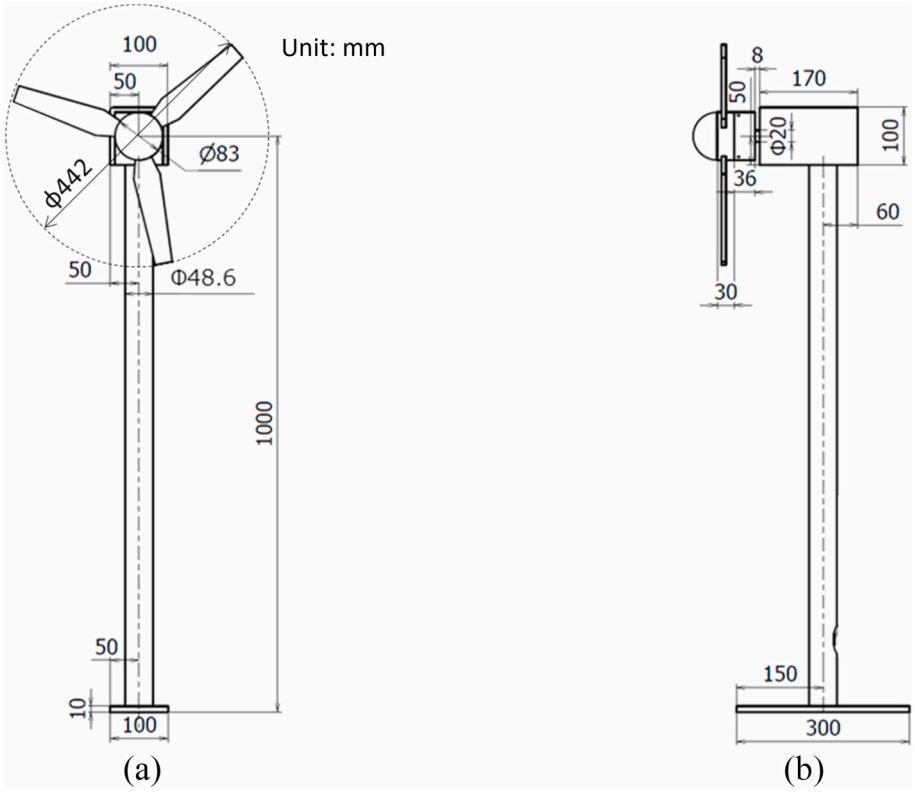

Fig. 5. Details of the wind turbine model: (a) front view, (b) side view.

2.2. Large-eddy simulations

To complementarily observe the flow field of the wake in the yaw state, numerical simulations were performed on the wind turbine model used in the wind tunnel experiments. This section describes the methodology of the numerical simulations.

2.2.1. Calculation methodology

In computational fluid dynamics (CFD), the finite difference method based on the Cartesian coordinate system is used to solve the flow field by applying LES to the turbulence model. LES applies a spatial filter to the flow field to model eddies with a sub-grid-scale (SGS) component that is smaller than the computational grid, while directly solving the simulation.

The governing equations of the flow field solved in this simulation are based on the continuity equation (Eq. (1)) and the Navier–Stokes equation (Eq. (2)) for an incompressible fluid expressed in tensor form (i, $j = 1, 2, 3$). The velocity and pressure fields are coupled using a partial-step method [30] based on the Euler explicit method. The Poisson equation for pressure is obtained by relaxation using the successive over-relaxation (SOR) method. The 3rd-order upwind scheme is used to discretize the convection term in Eq. (2), and the interpolation method of Kajishima [31] is used for the 4th-order central difference generated by the discretization of the convection term. The weight of the

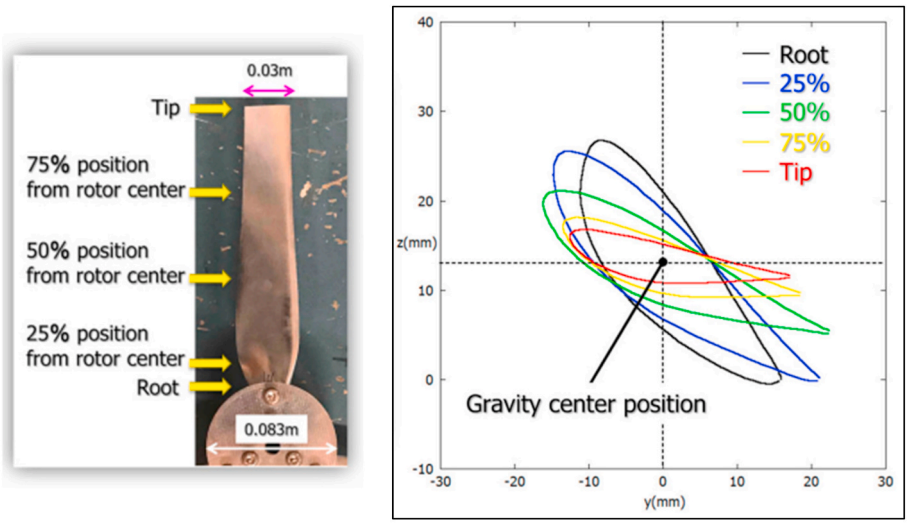

Fig. 6. Cross-section of the wind turbine blade at a typical radial position: (a) location of the displayed cross-section, (b) cross-sectional shape of the blade.

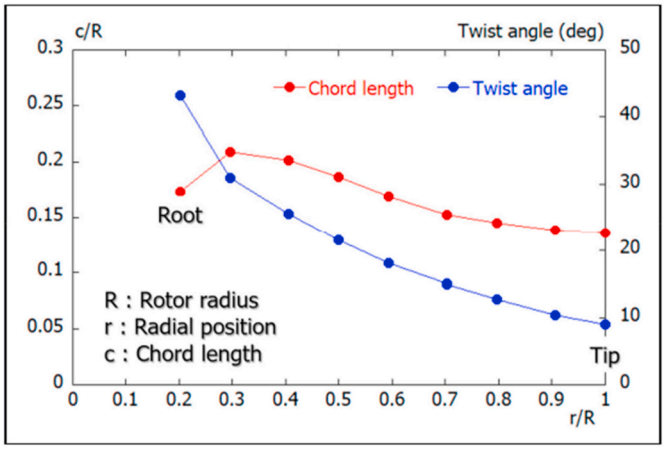

Fig. 7. Variations in the chord length and the twist angle from the root to the tip of the blade.

numerical viscosity term in the 3rd-order upwind scheme is generally set to 3.0 in the Kawamura–Kuwahara scheme [32], but in this study, it is set to 0.5 to sufficiently reduce its effect. For the other spatial terms, a 2nd-order central difference is applied.

The mixed time-scale (MTS) model proposed by Inagaki et al. [33] (Eq. (3)–(10)) is used to model the SGS component of the LES. The notation, (), denotes the filtering operator, for which the Simpson rule is adopted. Comparison of the LES solver used in this study with commercial Reynolds-averaged Navier–Stokes (RANS)-based CFD software (WindSim and Meteodyn WT) confirms that the LES solver can provide results comparable to CFD software [34].

In order to model the flow field of wind turbines, the actuator line model (ALM) was employed for the rotating turbine blades [35]. ALM approximates the volumetric forces acting on the fluid in the blades by lines, converting the tangential and thrust forces into volumetric forces acting in the flow and rotational directions, which are then added to the external force terms in the Navier-Stokes equations. The use of ALM enables detailed computation of the wind turbine wakes and significantly increases computation speed compared to CFD simulations of fully decomposed wind turbines that include a moving mesh. In this study, the rotational forces were decomposed into the spanwise and

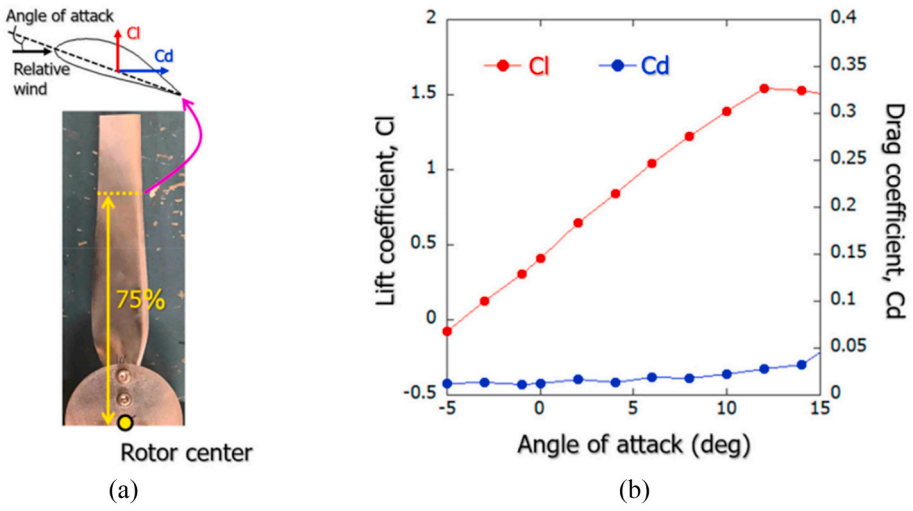

Fig. 8. Lift and drag coefficients against angle of attack in the blade cross-section at the 75% position from the rotor center: (a) 75% position in the image, (b) lift and drag coefficients.

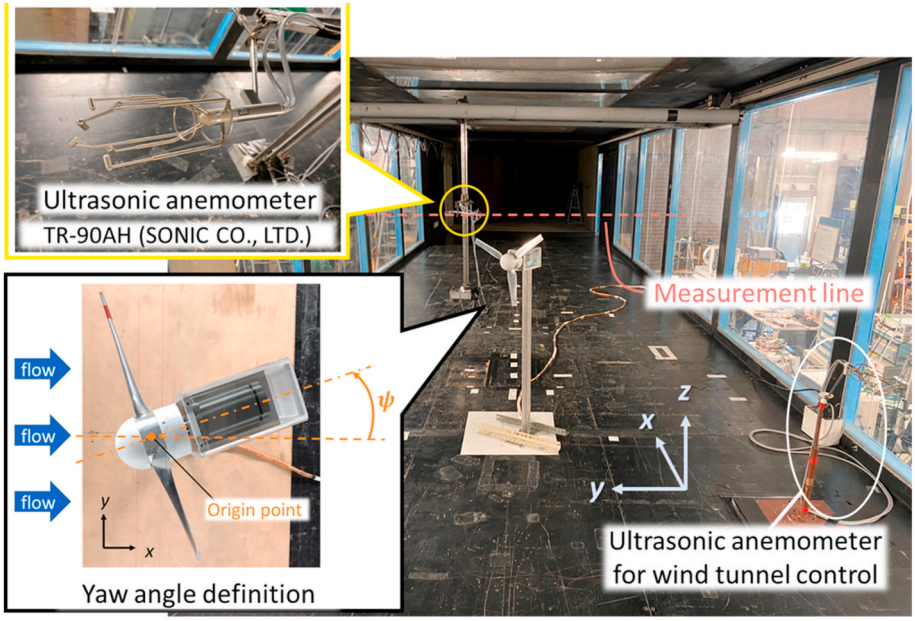

Fig. 9. Setup of the measurement equipment for the wind turbine wake.

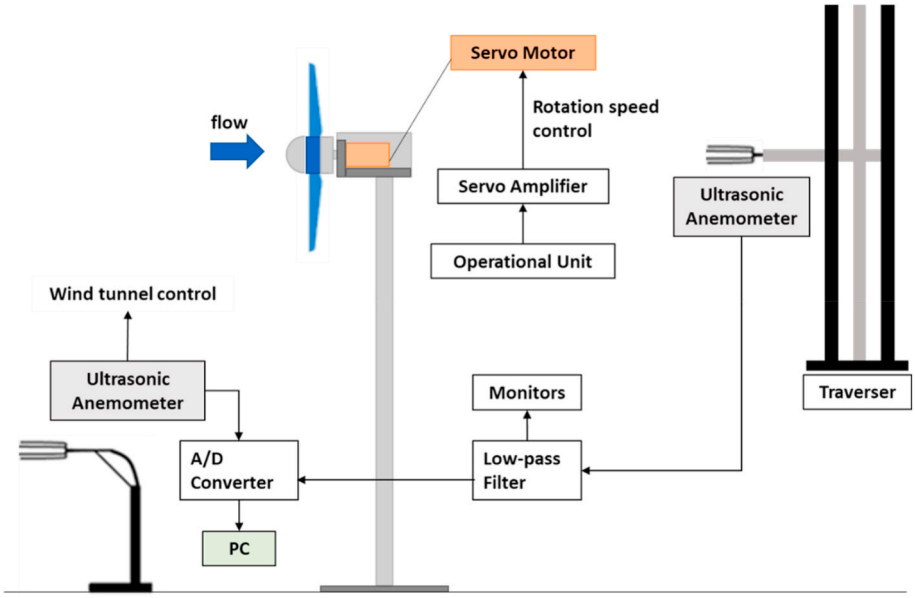

Fig. 10. Schematic diagram of the measurement system.

vertical directions and added to the external force term in the filtered Navier-Stokes equations (the fourth term on the right-hand side of Eq. (2)).

$$\frac{\partial \overline{u}_i}{\partial x_i} = 0 \tag{1}$$

$$\frac{\partial \overline{u}_i}{\partial t} + \overline{u}_j \frac{\partial \overline{u}_i}{\partial x_j} = -\frac{\partial \overline{p}}{\partial x_i} + \frac{1}{Re}\frac{\partial^2 \overline{u}_i}{\partial x_j \partial x_j} - \frac{\partial \tau_{ij}}{\partial x_j} + f_i \tag{2}$$

$$\tau_{ij} \approx \overline{u_i u_j} \approx \frac{1}{3}\overline{u_k u_k}\delta_{ij} - 2\nu_{SGS}\overline{S}_{ij} \tag{3}$$

$$\nu_{SGS} = C_{MTS} k_{es} T_s \tag{4}$$

$$C_{MTS} = 0.05 \tag{5}$$

$$k_{es} = (\overline{u}_k - \widehat{\overline{u}}_k)^2 \tag{6}$$

$$T_s^{-1} = \left(\frac{\Delta}{\sqrt{k_{es}}}\right)^{-1} + \left(\frac{C_T}{|\overline{S}_{ij}|}\right)^{-1} \tag{7}$$

$$|\overline{S}_{ij}| = \frac{1}{2}\left(\frac{\partial \overline{u}_i}{\partial x_j} + \frac{\partial \overline{u}_j}{\partial x_i}\right) \tag{8}$$

$$C_T = 10.0 \tag{9}$$

$$\Delta = (\Delta_x \bullet \Delta_y \bullet \Delta_z)^{1/3} \tag{10}$$

2.2.2. Calculation setup

The computational domain and the orthogonal staggered computational grid were set up as illustrated in Fig. 12. When calculating the

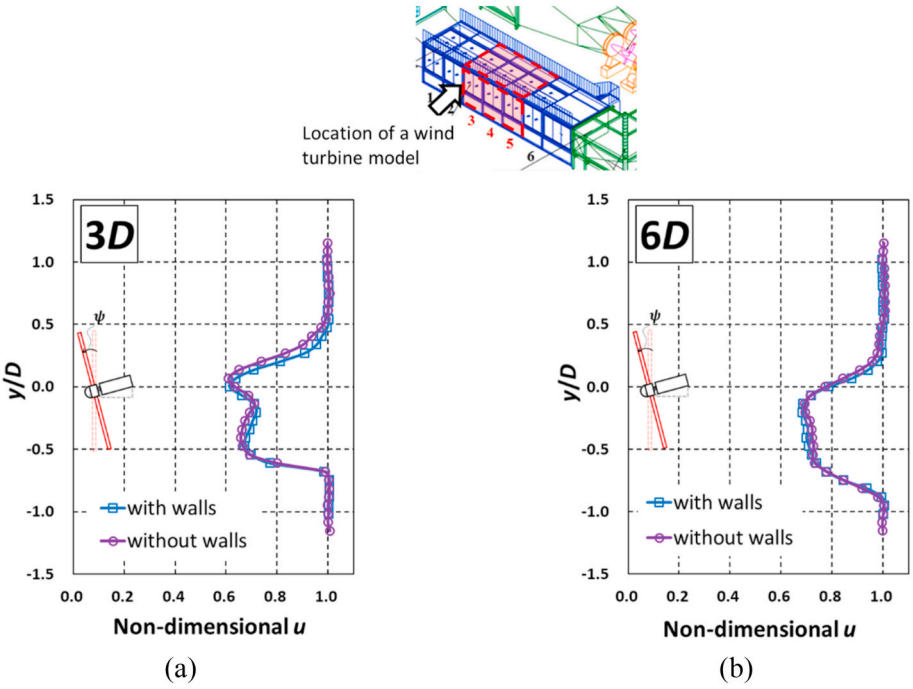

Fig. 11. Difference in time averaged non-dimensional velocity (= u/Uin) distribution of wind turbine wakes with and without wind tunnel walls in the yaw condition with $\psi = +30$deg: (a) at $x = 3D$, (b) at $x = 6D$.

wakes of the yaw state, the wind inflow into the computational domain was tilted to express the yaw state, as demonstrated in Fig. 13. The grid width downstream of the turbine was set to the minimum width for this calculation. The grid and wind turbine positions at $\psi = -30$ deg are shown in Fig. 13, but were mirrored to be symmetrical about the y-axis for the calculation at $\psi = +30$ deg. The output velocities were geometrically transformed according to the yaw angle of the incoming wind.

The computational domain was sized 11D, 9D, and 4.5D in the x-, y-, and z-directions, respectively, and the resolution of the minimum-width grid was 0.02D. The number of grid points for the inflow angle of 0° was 417, 291, and 133 for the x, y, and z directions, respectively, and the number of grid points for the yaw state was 417, 371, and 133 for the x, y, and z directions, respectively. The total number of grid points was 20.5 million.

The boundary conditions for the upper boundary and floor were set to the slip condition, while the lateral boundary had the Neumann condition, and the outflow boundary had the Sommerfeld radiation condition (SRC). Velocities were set to zero for all grid points contained within the nacelles and towers. The pressure boundary conditions were set to Neumann conditions at all boundaries. The dimensionless time increment based on the rotor diameter D and the inflow velocity Uin in the hub height was set to $\Delta t = 1 \times 10^{-3}$. Statistics were computed by time integration at dimensionless times $t = 21$ to 60.

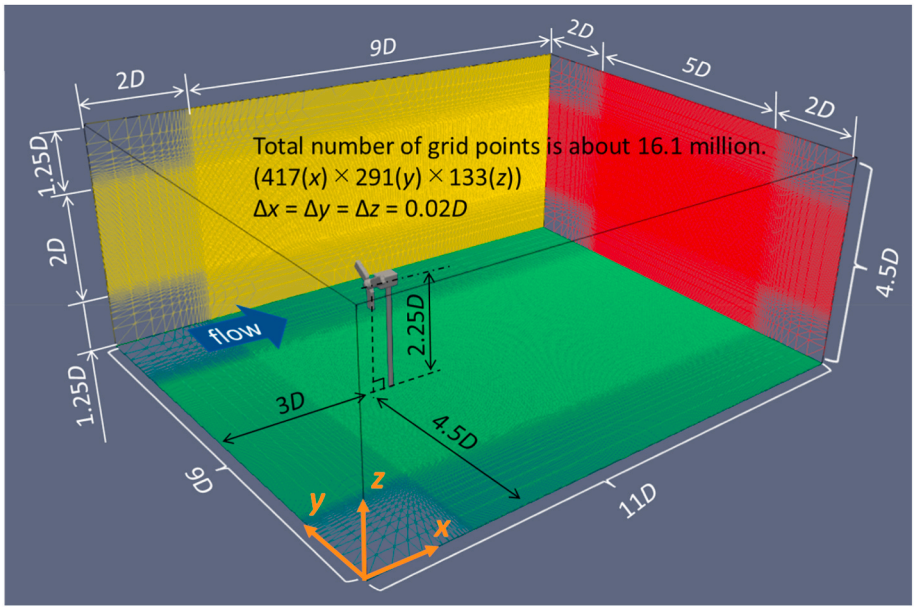

Fig. 12. Computational domain, grid and wind turbine positions set up in the simulation.

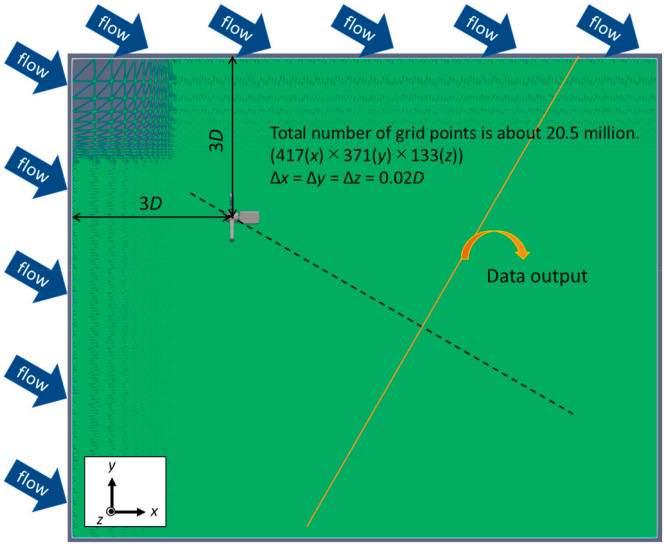

Fig. 13. Calculation grid set up for inclined incoming wind to represent relative yaw conditions.

3. Results and discussions

3.1. Wake horizontal distribution at the hub height

To confirm the left-right asymmetry of wake deflection in the yaw state, we investigated the horizontal distribution of hub height at $x = 3D$ and $6D$ downstream of the wind turbine for yaw angles $\psi = -30, -15, 0, +15, +30°$. The results for $\psi \geq 0$ are shown in Fig. 14(a), and for $\psi \leq 0$ in Fig. 14(b). Fig. 14(b) is presented with a larger vertical axis at the bottom of the graph, so that the direction of wake deflection on the paper is the same as in Fig. 14(a). The results in Fig. 14(a) and (b) indicate that, as the absolute value of the yaw angle increases, the wake deflects in the direction that the wind turbine is facing, and the velocity deficit becomes smaller.

The reason for the smaller velocity deficit in the yaw state is that the thrust force in the flow direction is decomposed into the flow direction and the lateral direction. For $\psi \geq 0$, the region of velocity deficit became narrower in the horizontal distribution of the wake hub height. Meanwhile, for $\psi \leq 0$, the wake was not deflected any further when the absolute value of the yaw angle was larger than 15°, confirming that the range of influence of the wake was wider in the horizontal distribution. In the present study, as in previous literature, we observed left-right asymmetry in both positive and negative yaw states of the wake.

3.2. Investigation of the cause of wake asymmetry occurrence

When the wind turbine was yawed at positive and negative angles, its

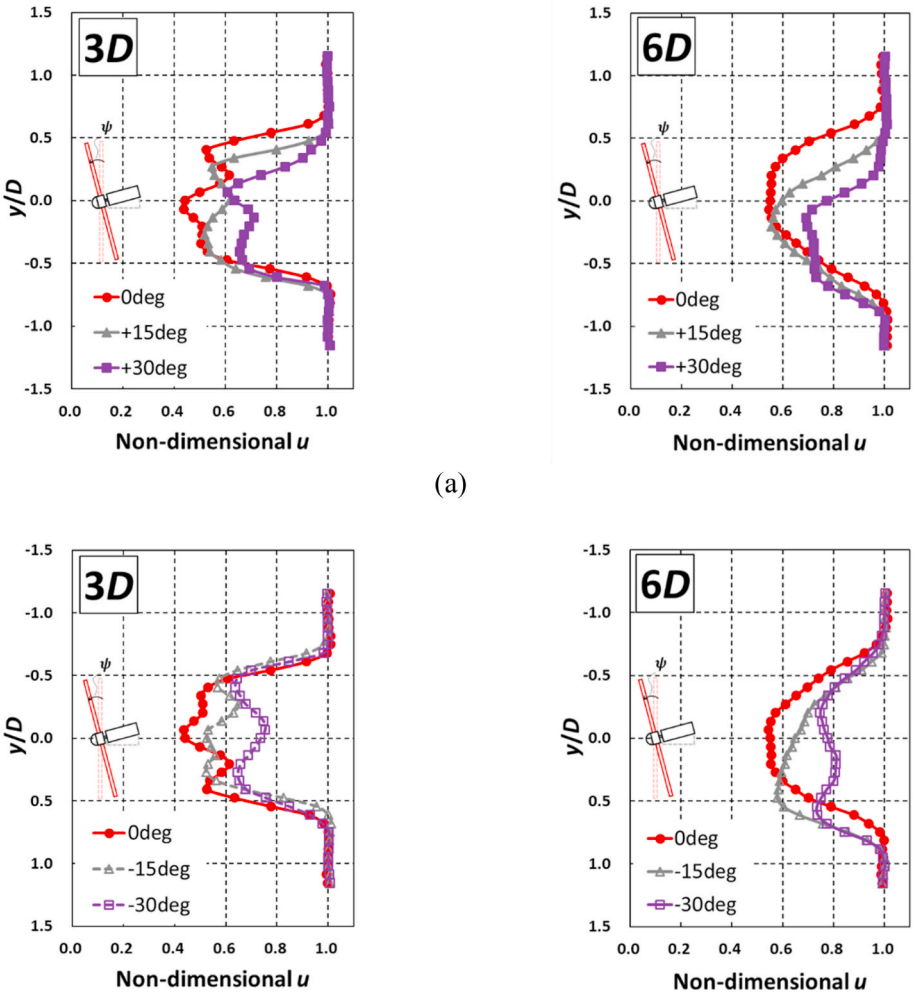

Fig. 14. Time-averaged velocity distribution of wind turbine wakes in the yaw state with (a) $\psi = 0, +15, +30$deg (b) $\psi = 0, -15, -30$deg at $x = 3D, 6D$.

orientation was symmetric about the x-axis in the main flow direction. Therefore, the wake profiles should have also been axisymmetric. However, as stated in Section 3.1, the profiles at ± yaw angles were different. To identify the source of wake asymmetry for positive and negative yaw conditions, this study builds on the work of Miao et al. [20] and focuses further on the interference between the wind turbine wakes and the bluff body in the yaw condition. Wind tunnel experiments were conducted to examine the bluff body condition, and the following three flow field measurements were taken. To complement these measurements, numerical simulations were also performed using LES.

I. Wake velocities u at the hub height were measured with the blades removed to obtain horizontal profiles in order to confirm the influence of the bluff body.
II. Wake velocities u were measured at the hub height and at $\pm 0.25D$ of the hub height, and the horizontal distributions were obtained to verify the difference in wake formation at the upper and lower regions of the rotor.
III. In order to isolate the influence of the blades on the wakes generated under different yaw conditions, the flow components u, v, and w above the rotor surface were measured at a distance of $x = 1D$ behind the wind turbine.

3.2.1. Confirmation of the effect of the object condition on wake asymmetry

Fig. 15 depicts the findings of Experiment I. Without blades, a velocity deficit was observed in the direction opposite to the wind turbine's tilt. When blades are present, the wakes deflect in the direction that the wind turbine faces due to the drag force on the fluid from the wind-receiving surface, which is in the same direction. The drag force is decomposed into flow direction and lateral direction, forming a wake behind the wind turbine with a velocity deficit in the flow direction, which is deflected by the lateral drag force. Without blades, the fluid experiences drag forces from the nacelle and the tower. The larger projected area of the nacelle causes greater lateral drag when viewed from the front, deflecting the wakes to the side with the larger projected area of the nacelle, i.e., opposite to the wind turbine's direction. The results with blades show that the wakes formed by the blades are more dominant in the wakes of wind turbines than in the wakes of nacelles, as the wind speed deficit at $y/D = 0.5$, which occurred in the condition without blades, is not observed. The profile of the negative yaw state's y-axis was inverted and plotted, and the profiles of the positive and negative yaw states were identical in the no-blade condition. This indicates that the wakes' horizontal profile's asymmetry in the yaw condition is caused by the wakes formed by the blades.

To investigate the influence of tower separation flow, numerical fluid flow simulations were conducted with and without the tower. The object conditions were changed as depicted in Fig. 16. The experimental and calculated results in the wind tunnel were compared in Fig. 17, which illustrates the horizontal distribution of wake velocity. The horizontal profile of wake velocity at $\psi = 0$ deg was in very good agreement between the experimental and simulated results, as shown in Fig. 17(a). The tower was found to cause asymmetry in the wake distribution to the left and right, as confirmed in the previous report by Kono et al. [26]. This shift was toward the direction of $y/D < 0$, as seen at $x = 3D$, as depicted in Fig. 18(a). While the previous study by Kono et al. [26] did not exactly match the results in Fig. 18(a), the study was modified to fit the experimental results of a wind turbine model [36], which has a different geometry than the current study. The simulation results with the tower in Fig. 16(b) and (c) reproduced the experimental results, with some deviations. Notably, the difference between the horizontal distributions at $\psi = +30$ deg, confirmed by the experimental results, and the inverted horizontal distribution at $\psi = -30$ deg were reproduced. The simulation results in Fig. 18(b) by Miao et al. [20] show good agreement with both the experimental and simulation results in this study in terms of trend for the wind speeds of $\psi = -30$, $+30$, and 0 deg in increasing order.

Comparing the horizontal profiles with and without the tower, the horizontal profiles of wake velocity matched in the positive and negative yaw conditions without the tower. These results, combined with those from wind tunnel experiments with blades removed, suggest that the asymmetry of wakes in the positive and negative yaw conditions is caused by both the flow formed by wind turbine blades and the effect of the wind turbine tower.

3.2.2. Wake horizontal distribution at the three heights

Experiments conducted by Pierella and Saetran [25] have demonstrated that wind turbine wakes are deflected vertically downward due to interference with tower separation flow. Therefore, in this study, in addition to the hub height, horizontal distributions were obtained for each height that is $\pm 0.25D$ of the hub height. Fig. 19 shows the measurement positions and results of Measurement II. Figs. 20–22 display

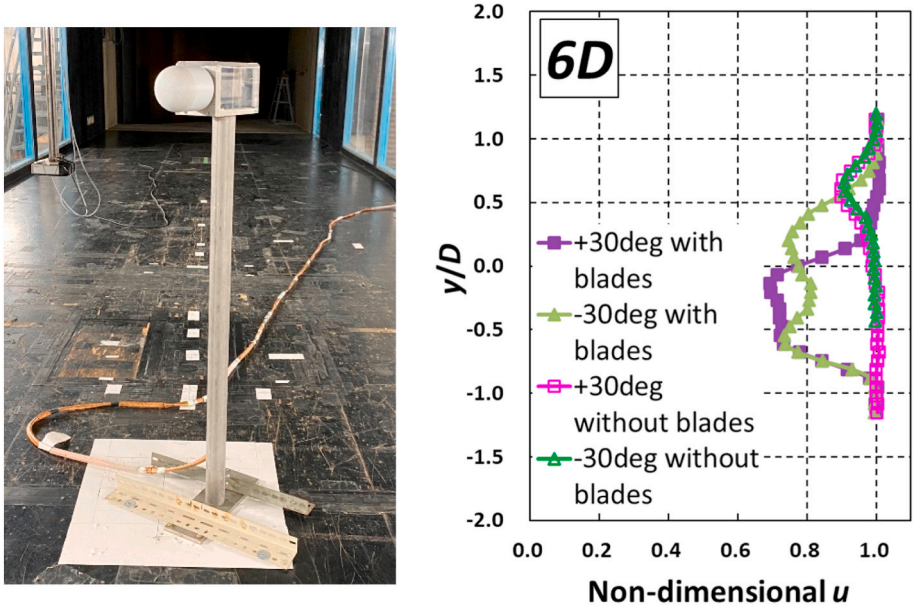

Fig. 15. Difference in horizontal distribution of wake velocity with and without turbine rotors.

Fig. 16. Object conditions set by computed fluid dynamics simulation: (a) with a tower, (b) without a tower.

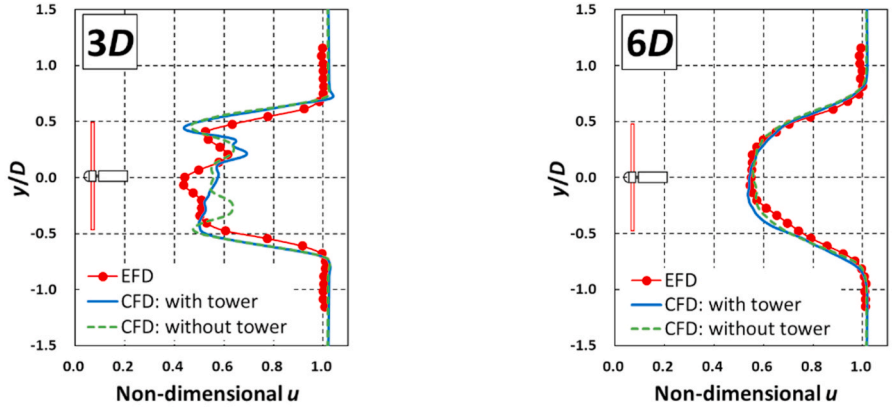

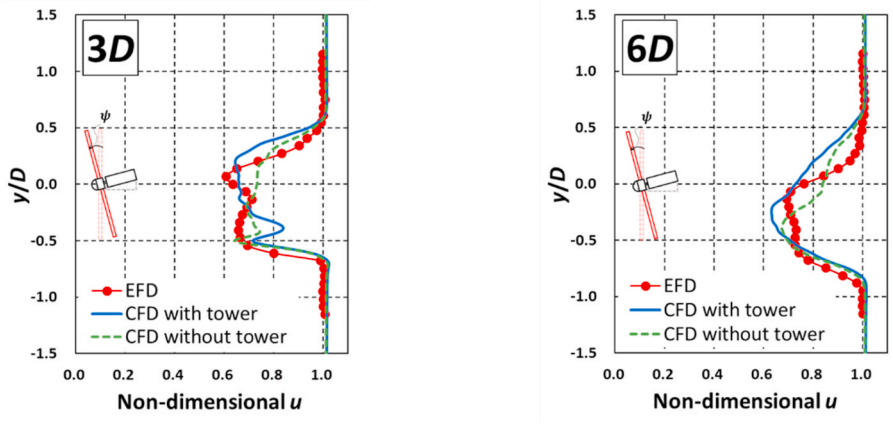

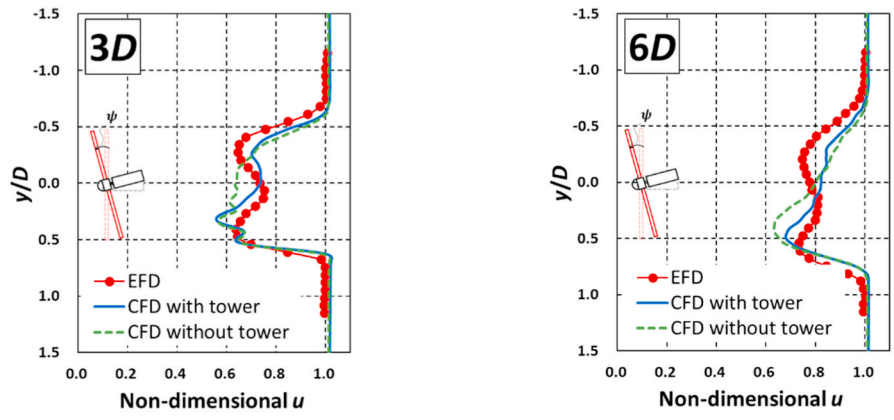

Fig. 17. Comparison of horizontal profiles of time-averaged velocities at hub height for different bluff body conditions: (a) $\psi = 0$ deg (b) $\psi = +30$ deg, (c) $\psi = -30$ deg.

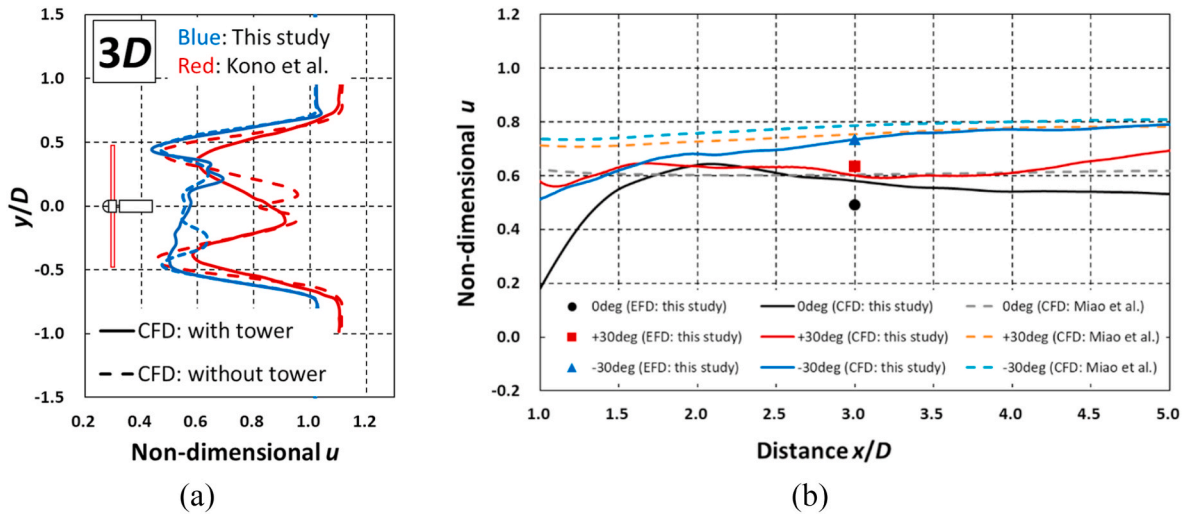

Fig. 18. Comparison with previous works; (a) Wake horizontal profile with different object conditions [26], (b) Velocity deficit versus distance by yaw state [20].

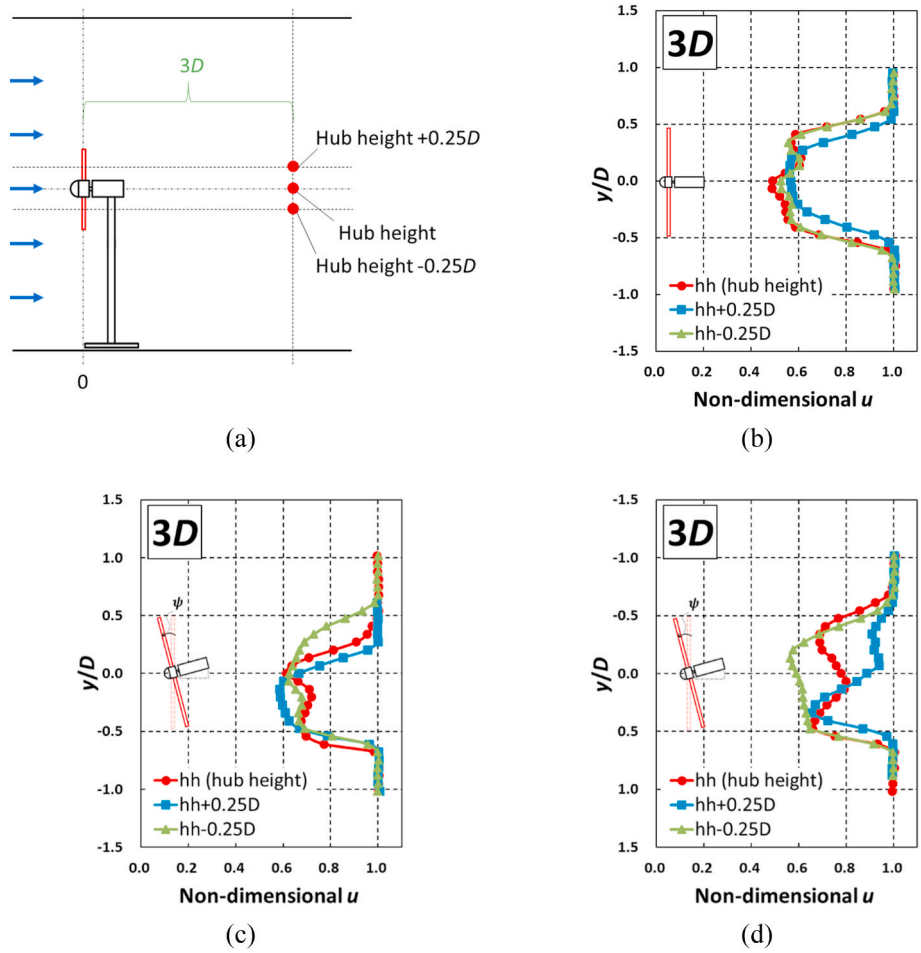

Fig. 19. Horizontal distribution of wake velocities at hub height $\pm 0.25D$ at $x = 3D$: (a) Measurement position, (b) Result with $\psi = 0$ deg, (c) Result with $\psi = +30$ deg, (d) Result with $\psi = -30$ deg.

the visualization of the horizontal cross-sectional flow field at different heights from the LES results for different object conditions. The color plot of the instantaneous field at dimensionless time $t = 30$ indicates the flow velocity in the flow direction, and the black line in the figure shows the isopleth $\nabla^2 p = \partial p/\partial x + \partial p/\partial y + \partial p/\partial z$ of the Laplacian of pressure $\nabla^2 p = 20$. The pressure Laplacian can visualize areas of rapid physical change, and in the figure, the tip vortex and the detached vortex from the bluff body were captured.

Experimental results in Fig. 19(b) show that at yaw angle $\psi = 0$ deg, the horizontal profile obtained at hub height $+0.25D$ is axisymmetric, whereas at hub height and below hub height, the velocity deficit in the profile is biased toward the negative side of the vertical axis. This result

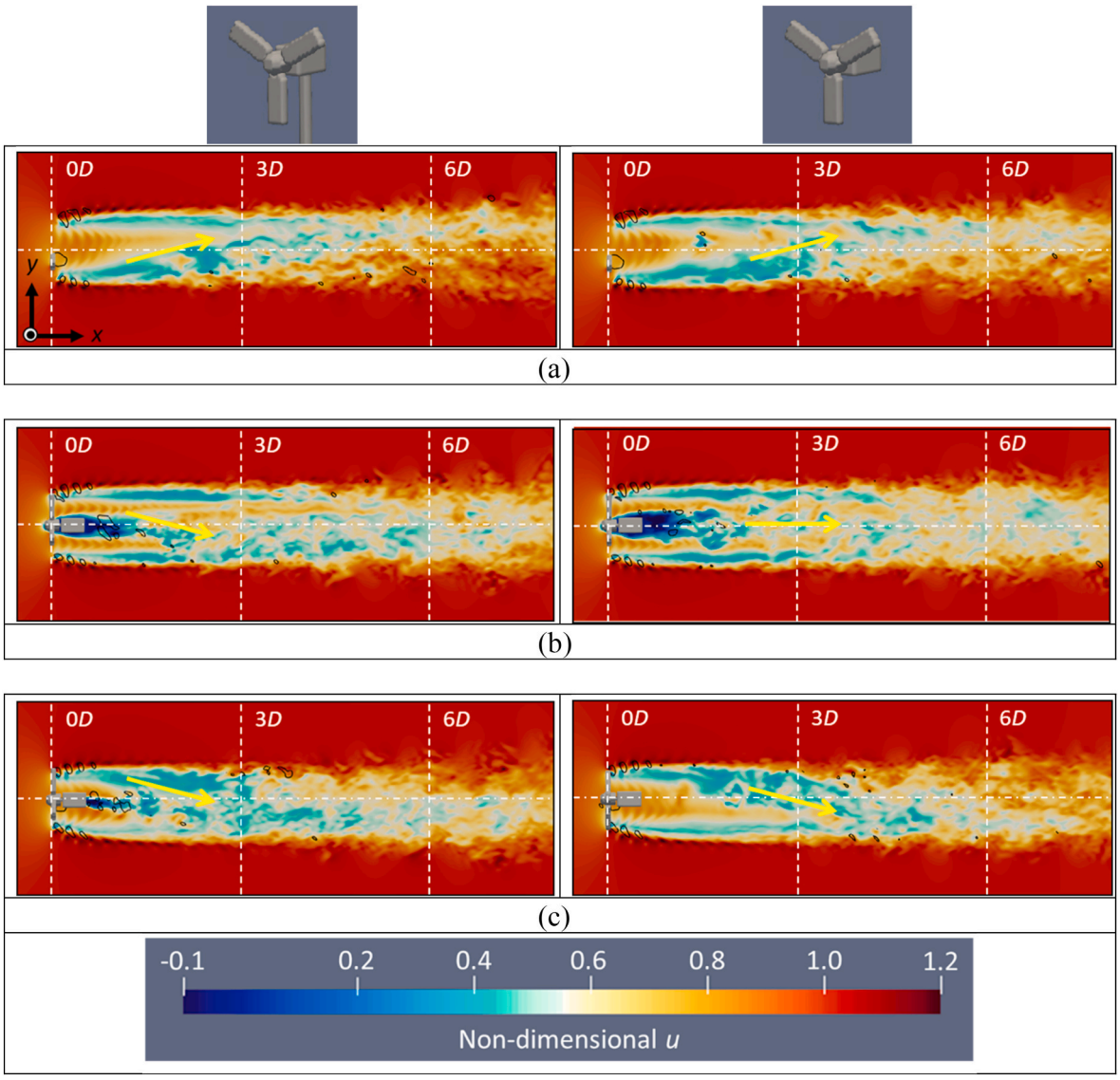

Fig. 20. Instantaneous field at dimensionless time $t = 30$ of numerical simulation results of flow velocities in the direction of flow on horizontal cross sections at three heights when $\psi = 0$ deg (comparison by object condition): (a) at the height of hub height+0.25D, (b) at hub height, (c) at the height of hub height–0.25D.

was also confirmed by simulations conducted by Kono et al. [26], who concluded in a previous study that the turbulence was due to transport by tower effects. In the present study, it was experimentally confirmed that the asymmetry of the wakes is manifested by the effect of the towers. Focusing on the maximum wind velocity deficit, the largest deficit was observed at the hub height, and the magnitude of the deficit was different above and below the hub height. As reported by Pierella and Saetran [25], it is inferred that the maximum wind speed deficit was caused by the vertical downward wake deflection due to the tower detachment flow, which was advected below the hub height.

From Fig. 20(b) of the simulation results for $\psi = 0$ deg, a comparison of the flow field at the hub height for the with-tower and without-tower conditions shows that the flow field for the without-tower condition is straight downstream of the flow deduced by the nacelle, while the flow field for the with-tower condition is deflected downward on the paper. Fig. 20(a) and (c) show that the flow field is symmetrical about the flow direction axis at the hub height of $\pm 0.25D$ in the condition without tower, but in the condition with tower, the flow field above the hub height is different due to the interference of the tower separation flow with the blades wakes. Similar to the nacelle peeling flow, the tower peeling flow was also deflected downward from the paper surface. From these simulation results, it is evident that the tower is a contributing factor to the asymmetry of the flow field, and it was observed that the separation flow from the nacelle and tower deflects in the negative y-axis direction defined in this study.

Fig. 19(c) indicates that the maximum velocity deficit above the hub height was greater than the deficit at the hub height when $\psi = +30$ deg. Conversely, below the hub height, the amount of loss remained the same, and the wake range became wider. Moreover, in Fig. 19(d) at $\psi = -30$ deg, the range of the wake loss was significantly smaller above the hub height, whereas both the amount and range of the wake loss were larger below the hub height. It was initially expected that the velocity distributions would be the same between positive and negative yaw states above the hub height, as the tower's separation flow does not interfere with the flow field. However, this was not the case, and at $\psi = +30$ deg, a narrow range of strong velocity deficits was measured, while at $\psi = -30$ deg, a wide range of weak velocity deficits was observed. This is believed to be due to the difference in the strength of the wake velocity deficits formed above and below the hub height in the yaw state. Consequently, it is inferred that there is a variation in the shape of the velocity distribution above the hub height for $\psi = \pm 30$ deg. By comparing the LES results of (a) and (c) in Fig. 21 and (a) and (c) in

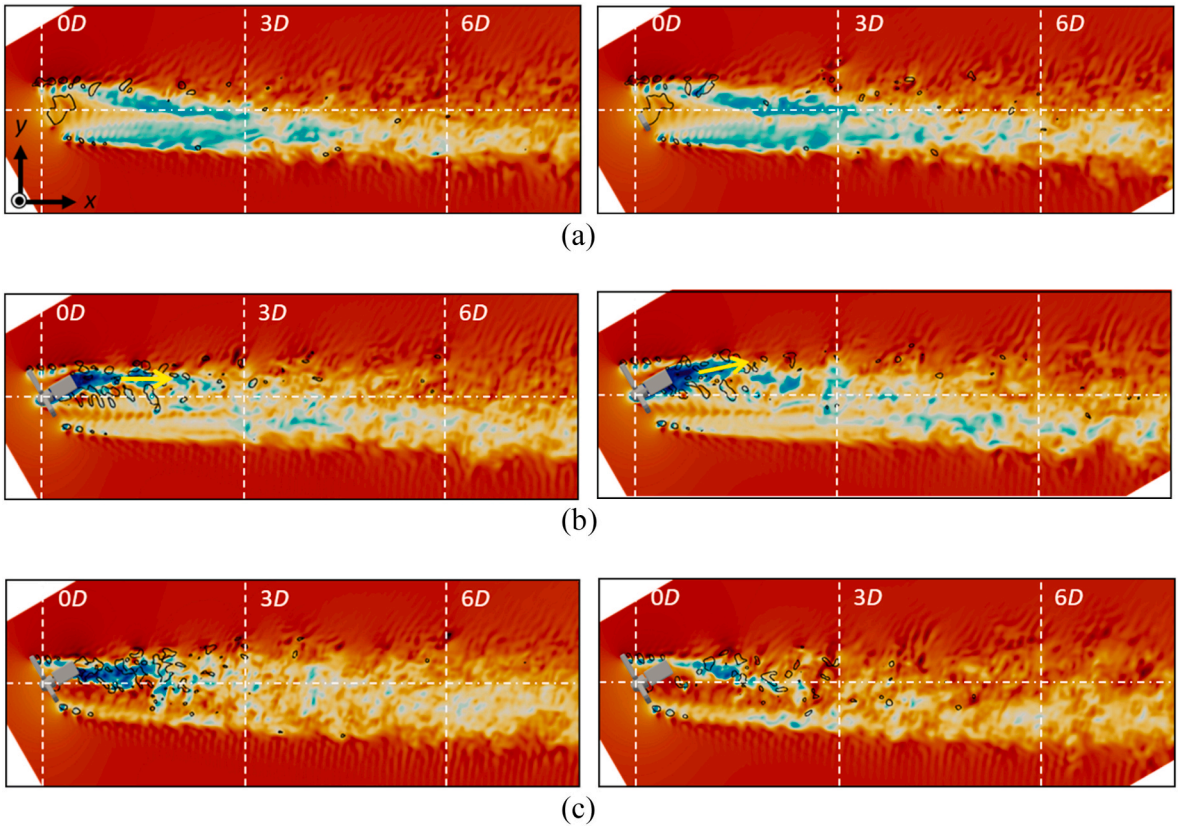

Fig. 21. Instantaneous field at dimensionless time $t = 30$ of numerical simulation results of flow velocities in the direction of flow on horizontal cross sections at three heights when $\psi = +30$ deg (comparison by object condition): (a) at the height of hub height+0.25D, (b) at hub height, (c) at the height of hub height–0.25D.

Fig. 22 for the no-tower condition, The flow fields at the hub height $+0.25D$ for $\psi = +30$ deg and $-0.25D$ for $\psi = -30$ deg, as well as the flow fields at the hub height $-0.25D$ for $\psi = +30$ deg and $+0.25D$ for $\psi = -30$ deg, exhibited axisymmetry. Furthermore, it was found that in each yaw state, the flow field is not axisymmetric between the upper and lower hub heights. This indicates that there is vertical asymmetry in the wake of the wind turbine in the yaw state, regardless of the presence of the tower. Focusing on the angle of attack with respect to the flow velocity into the blade, it can be understood that the angle of attack of the blade at the top end of the wind turbine in the yaw state is different for each blade rotation angle because the yaw angle of the wind turbine is added (or subtracted) to the blade attachment angle. In other words, for a wind turbine in yaw, the blade attachment angle is plus (or minus) a value related to the wind turbine yaw angle at the top of the hub height and minus (or plus) at the bottom. Fig. 8(b) shows that the lift and drag forces generated by the blades change with the angle of attack of the flow to the blades, and the strength of the wakes formed at the upper and lower hub heights differs in the yaw state. Similar to the simulation results obtained without a tower, the flow field shaped by these wakes exhibits substantial dissimilarities between the upper and lower hub heights.

Comparing the flow fields at the hub height for the results with $\psi = \pm 30$ deg from LES results Figs. 21(b) and Fig. 22(b), it can be observed that the detached flow in the nacelle with tower condition is deflected downward on the paper compared to the without tower condition, but the difference is not as pronounced as in the results for $\psi = 0$ deg.

3.2.3. *Wake structure in the near-wake region seen from behind a wind turbine*

Fig. 23 and Table 1 illustrate the measurement positions and results of Experiment III, respectively. The velocity vectors in the y-z plane in Fig. 23 were derived using the data from Table 1. The figure shows that for $\psi = 0$ and -30 deg, the flow was formed along the direction of rotation, while there was almost no lateral flow for $\psi = +30$ deg. Behind the wind turbine, the fluid was subjected to a reaction from the blade rotation and formed a swirling flow in the direction opposite to the blade rotation. As the fluid was also pushed in the direction the wind turbine was facing in the yaw state, it was concluded that the swirling flow and the flow generated at the rotor of the wind turbine canceled each other at $\psi = +30$ deg, resulting in the absence of turning flow (flow in the positive y-axis direction). In Table 1, the flow velocity in the flow direction was found to be higher at $\psi = -30$ deg than in the other two cases. At $\psi = -30$ deg, the blade rotated towards the incoming wind when the blade was positioned at the top edge, causing the attack angle of the blade to decrease and the lift and drag coefficients to increase compared to the other two cases. Thus, the lift and drag coefficients at the top of the rotor were lower, resulting in weaker wake formation than in the other cases. Conversely, at $\psi = +30$ deg, the flow velocity in the flow direction remained unchanged compared to $\psi = 0$ deg, suggesting that the wake in the upper part of the rotor was actively formed.

In section 3.2.2, it was confirmed that the flow fields at hub height $+0.25D$ and hub height -0.25D for $\psi = +30$ deg, as well as the flow fields at hub height $-0.25D$ and hub height $+0.25D$ for $\psi = -30$ deg, are symmetrical under the condition without a tower. In other words, based on the results of this experiment and section 3.2.2, it can be inferred that for $\psi = +30$ deg, the mainstream velocity in the upper part of the swept area is lower, as well as the swirling flow, while in the lower part of the swept area, the opposite is true. Similarly, for $\psi = -30$ deg, it can be inferred that the mainstream velocity and swirling flow are higher in the upper part of the swept area, while the opposite is true in the lower part.

Fig. 24 illustrates a contour plot that visualizes the time-averaged velocity in the main flow direction behind the wind turbine, based on the calculated yaw state for $\psi = 0$, $+30$, and $-30°$. The contour line where the velocity in the main flow direction $u = 0.5$ is shown in white,

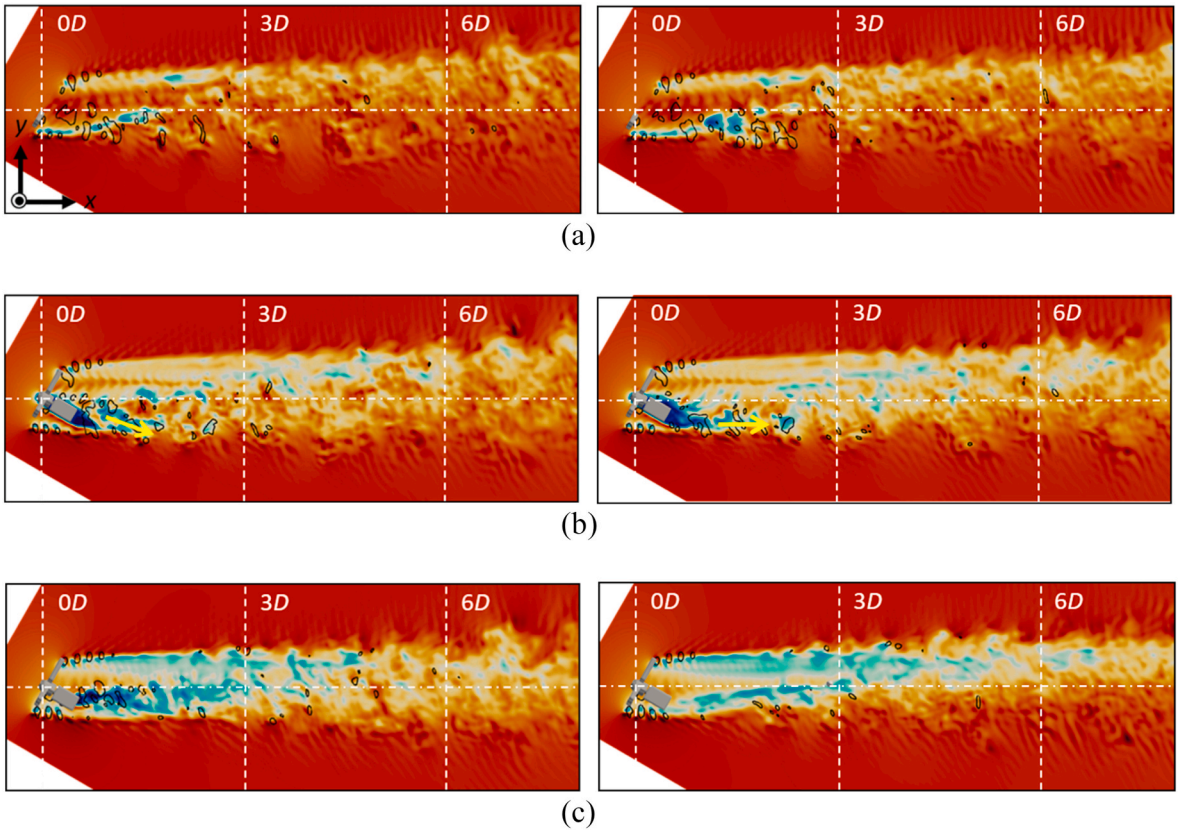

Fig. 22. Instantaneous field at dimensionless time t = 30 of numerical simulation results of flow velocities in the direction of flow on horizontal cross sections at three heights when $\psi = -30$ deg (comparison by object condition): (a) at the height of hub height+0.25*D*, (b) at hub height, (c) at the height of hub height–0.25*D*.

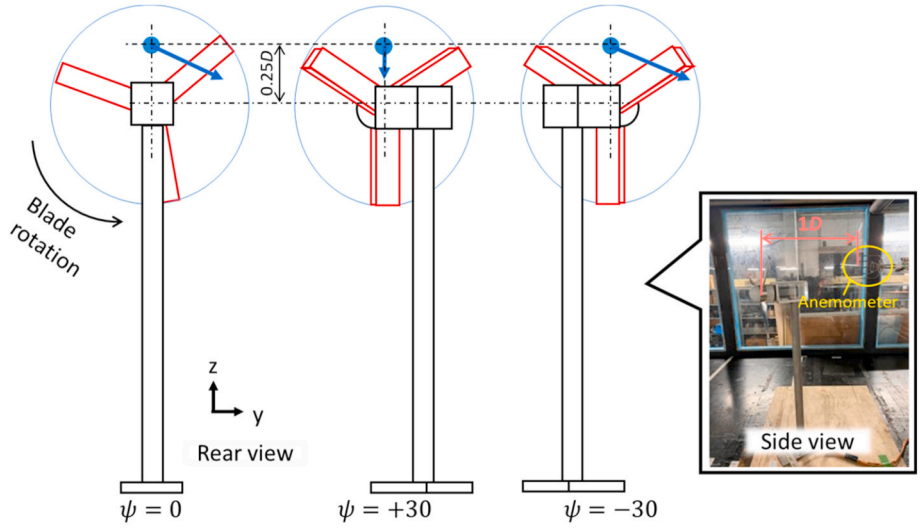

Fig. 23. Measurement position and measured vector of flow formed by blades.

Table 1
Measurement results of flow formed by blades.

ψ deg	u/U_{ref}	v/U_{ref}	w/U_{ref}	$\sqrt{v^2+w^2}$	$\tan^{-1}(w/v)$
0	0.63	0.13	−0.06	0.14	−24.78
+30	0.60	0.00	−0.06	0.06	−90.00
−30	0.79	0.14	−0.06	0.15	−23.20

and the flow vectors are indicated by white arrows. The upper left of the figure displays the separation distance in the flow direction from the rotor center position. The top row of the figure shows the results with the tower, while the bottom row shows the results without tower. At $\psi = 0$, the wake swirling counter to the blade rotation is visible, and for both conditions, the shape of the wake distorts as one moves away from the wind turbine, and the wake wind speed recovers as it mixes with the flow around the wake.

Fig. 24(a) demonstrates that the flow field without a tower at $\psi = 0$ is point-symmetric with respect to the hub center. On the other hand, with

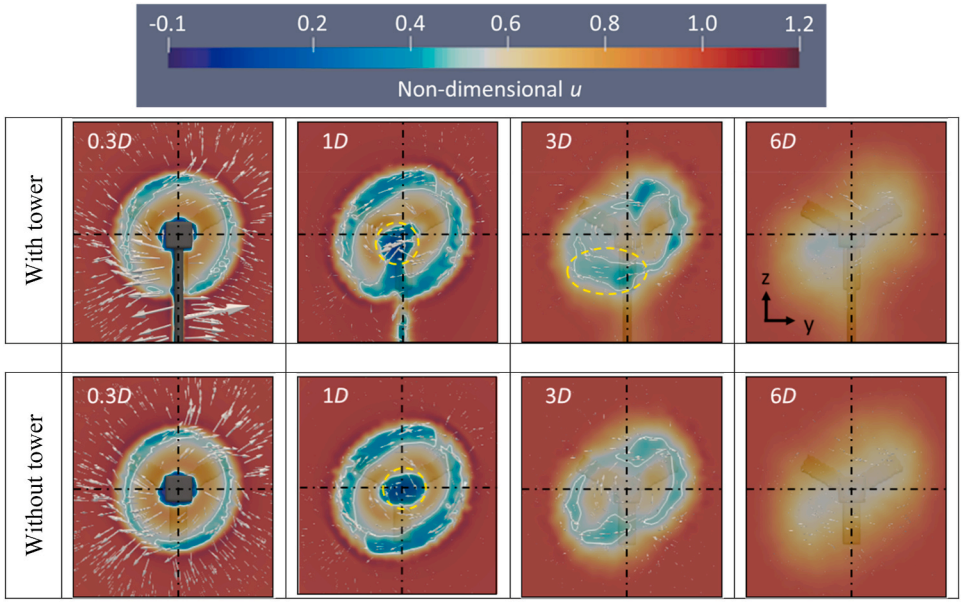

(a)

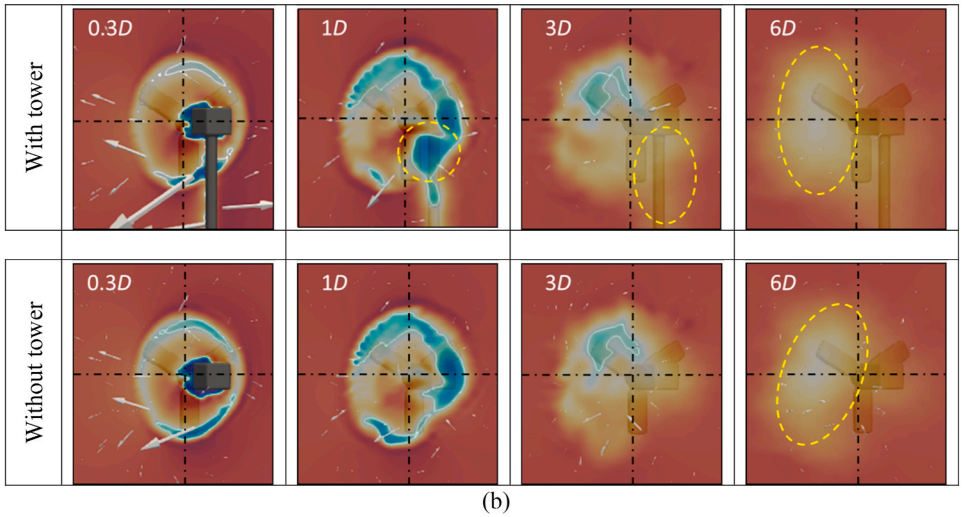

(b)

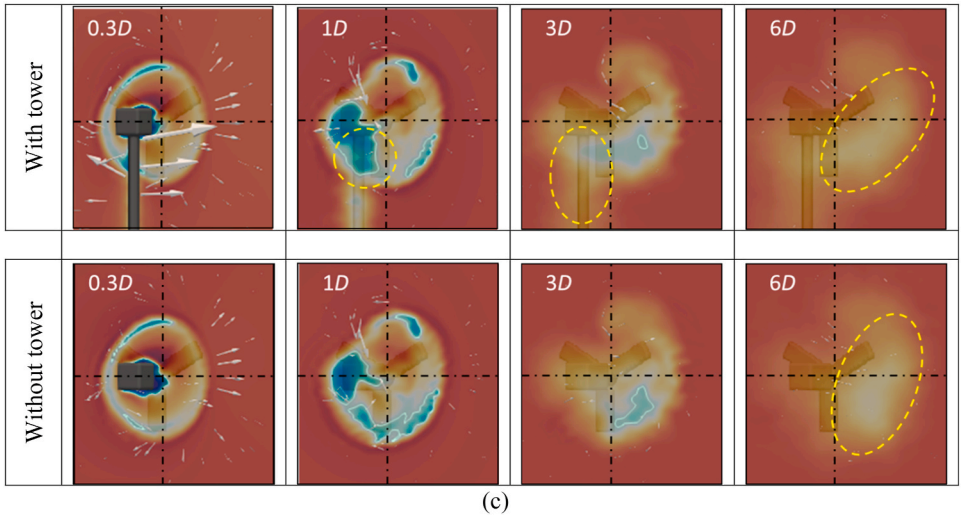

(c)

Fig. 24. Comparison of contour plots of time averaged velocity viewed from directly behind the wind turbine for each object condition (upper panel with tower, lower panel without tower): (a) $\psi = 0$deg, (b) $\psi = +30$deg, (c) $\psi = -30$deg.

the tower, the flow field is not point-symmetric due to the presence of tower separation flow. The figure is divided into four regions by vertical and horizontal planes relative to the hub center. By comparing the magnitudes of the vectors in the upper right and lower left of the figure, the lower left vector is larger in the flow field at $x = 0.3D$. It is assumed that the presence of the tower causes this difference due to the increased velocity of the flow between the rotor surface and the tower. When comparing the flow field at $x = 1D$, the nacelle separation flow was located in the center of the figure in the condition without the tower, whereas in the condition with the tower, it was advected to the lower left of the four regions. Detailed observation of the condition with the tower revealed that when the nacelle separation flow is deflected vertically downward by the tower separation flow, the nacelle separation flow is diverted to the lower left due to interference between the swirling flow formed behind the wind turbine and the nacelle separation flow. The results show that at $x = 3D$ and $6D$, the wind turbine wake is not only deflected vertically downward but also advected down to the left behind the wind turbine. Based on these results, it is believed that the phenomenon of the nacelle and tower separation flow deflecting in the negative y-axis direction, as confirmed in section 3.2.2, is caused by the transport of the nacelle and tower separation flow by the swirling flow.

Fig. 24(b) display the results of the yaw condition at $\psi = +30$ deg with and without a tower, respectively. Unlike the results for $\psi = 0$ deg, the swirl flow was not observed in the yaw condition at $\psi = +30$ deg. The yaw steering deflected the wake to the left side of the plot, resulting in a smaller vector in the upper part of the figure at $x = 0.3D$ compared to $\psi = 0$ deg, while it was larger in the lower part of the figure. This is consistent with the results of Measurement III. At $\psi = +30$ deg, a velocity deficit due to the wake was observed in the upper part of the figure. The difference in the magnitude of the rotation vector at the top and bottom of the wake, and the difference in the velocity in the flow direction, are assumed to be the causes of the failure to maintain the swirling flow. Therefore, unlike the case of $\psi = 0$ deg, it is believed that in the flow field at the hub height, there was no deflection of the nacelle and tower separation flow in the negative y-axis direction. Comparing the flow fields for the conditions with and without the tower, it can be seen that in the condition with the tower, the yellow dotted line in the figure for $x = 1D$ shows a decrease in flow velocity, indicating the appearance of the tower effect. In the lower-left region of the figure, the velocity deficit of the annulus at the wing tip was maintained without the tower, whereas the annulus collapsed with the tower. After $x = 1D$, the velocity deficit caused by the tower's detached vortex, enclosed by the dotted yellow rectangle, has a clear effect on the flow field with the tower, and the wake in the nacelle area behaved as if it were being pulled downward, as in the case of $\psi = 0$ deg. At $x = 6D$, the slope of the dotted yellow ellipse surrounding the main wake is different from that in the no tower condition due to the tower separation flow, indicating that the shape of the wake is clearly different with and without the tower.

In Fig. 24(c), no clear swirling flow was observed for the yaw condition at $\psi = -30$deg, similar to the case at $\psi = +30$ deg. However, the slope of the yellow dotted ellipse differed between conditions with and without a tower, due to the tower separation flow effect. Nevertheless, there was a velocity deficit due to wakes in the lower part of the figure, contrary to the case of $\psi = +30$ deg. Consistent with Measurement III of the wind tunnel experiment, a larger velocity deficit was observed on the upper side of the rotor surface in the yaw condition of $\psi = +30$ deg, while a larger velocity deficit was observed below the rotor for the yaw condition of $\psi = -30$ deg. Moreover, the wake distribution was opposite in the vertical direction for the positive and negative yaw conditions without the tower. In the presence of the tower, the wakes of the blades concentrated in the upper left, and the tower separation flow formed in the lower right interfered with each other in the yaw state of $\psi = +30$ deg, resulting in the wakes of the entire wind turbine expanding vertically. On the other hand, in the yaw condition of $\psi = -30$ deg, the wakes of the blades concentrated in the lower right, and the tower separation flow formed in the lower left interfered with each other, resulting in the wakes of the entire wind turbine expanding laterally.

4. Conclusions

To investigate the wakes of a wind turbine with the wake steering technique applied in more detail, we conducted wind tunnel experiments using a wind turbine model and large-eddy simulations to focus on the interference with the bluff body. In the wind tunnel experiments, differences in the horizontal distribution of the wake velocity at the hub height were observed in positive and negative yaw conditions, and three experiments were conducted to confirm the tower effect. In the LES, which accurately replicates the wind turbine model, the wakes of the wind turbine formed in each yaw state of $\psi = 0$, $+30$, and -30 deg were computed for the object conditions with and without the tower, and their flow fields were visualized and compared.

Similar measurements of wake velocity with the blades removed from the wind turbine model showed that the horizontal distribution of the hub height was symmetrical in positive and negative yaw conditions, indicating that the asymmetry of the wakes was due to blade rotation. The LES results for the conditions with and without the tower showed that the horizontal distributions in the positive and negative yaw states coincided in the condition without the tower, confirming that the deformation caused by blade rotation and the effect of the tower interfere with each other and cause symmetry in the horizontal distributions in the positive and negative yaw states.

Wake velocity measurements were taken at three different heights, and a clear difference in horizontal distribution was observed above and below the hub height. At $\psi = 0$ deg, the wakes of the wind turbine were found to be advected vertically downward due to the tower. At $\psi = +30$ deg, the maximum velocity deficit on the upper side of the rotor was larger than the deficit at the hub height, while the maximum velocity deficit on the lower side of the rotor was larger than the deficit at the hub height. However, at $\psi = -30$ deg, the deficient area on the upper side of the rotor was significantly narrower than the deficit at the hub height, while both the deficient amount and the deficient area on the lower side of the rotor were larger than the deficit at the hub height. Upon observing the results of the LES, it was confirmed that the nacelle and tower separation flow is deflected in the negative y-axis direction when $\psi = 0$, but this phenomenon was rarely observed at $\psi = \pm 30$deg. Furthermore, the flow fields at hub height $+0.25D$ for $\psi = +30$ deg and hub height $-0.25D$ for $\psi = -30$ deg, as well as the flow field at hub height $-0.25D$ for $\psi = +30$deg and hub height $+0.25D$ for $\psi = -30$ deg, exhibited axisymmetric characteristics. It was found that the flow fields at the upper and lower sides of the hub height were not axisymmetric in each yaw state, and asymmetry in the wind turbine wake existed vertically regardless of the presence of the tower.

After conducting wake measurements at the top of the rotor to analyze the blade-only wake, it was found that the flow-directional velocity was greater at $\psi = -30$ deg. The angle of attack of each blade at the top of the wind turbine in the yaw state varies due to the addition (or subtraction) of the yaw angle of the wind turbine to the blade mounting angle, resulting in different lift and drag for each blade rotation angle. As a result of the smaller angle of attack of the blade at the top of the rotor at $\psi = -30$ deg, it can be inferred that the flow direction velocity at the top of the rotor increased during the yaw condition at $\psi = -30$ deg. The increase in flow velocity in the turning direction can be attributed to the alignment between the lateral resistance caused by the tilted wind turbine and the direction of the turning flow. On the other hand, at $\psi = +30$ deg, the flow velocities in the main flow direction and the turning direction decreased at the upper part of the rotor.

To understand the asymmetry of the wake caused by the interference phenomenon between the tower and the wind turbine wake, the LES results were analyzed in detail from behind the turbine. For $\psi = 0$ deg, the detached flow from the tower caused the vertical downward advection of the wind turbine wake. The nacelle separation flow was also displaced from the center of the swirling flow of the wake, causing it

to flow to the left from behind the wind turbine. This captures the mechanism by which the wake is not symmetrical in the no yaw misalignment condition. With respect to the yaw state, it was observed that the velocity deficit was larger on the upper side of the rotor surface for the yaw state of $\psi = +30$ deg, and conversely, the velocity deficit was larger on the lower side of the rotor for the yaw state of $\psi = -30$ deg. In the yaw condition, the diagrammatic vector was larger in the area where the direction of the wake deflection by yaw steering coincided with the direction of the wake turn, and smaller in the area where the directions did not coincide, compared to the case of $\psi = 0$ deg. In the yaw conditions of $\psi = +30$ and -30 deg, the swirling flow that was clearly visible when $\psi = 0$ deg could not be observed. This is due to the difference in the magnitude of the rotation vectors at the top and bottom of the wake and the difference in the velocity in the flow direction, which prevented the swirling flow of the formed wake from being maintained. In the without tower condition, the wakes were opposite in the vertical direction for the positive and negative yaw conditions. In the case of the tower, in the yaw state of $\psi = +30$ deg, the wakes of the blades concentrated in the upper left and the tower separation flow formed in the lower right interfered with each other, and the overall wakes of the wind turbine widened vertically. In the yaw condition of $\psi = -30$ deg, the wakes of the blades concentrated in the lower right and the tower shedding flow formed in the lower left interfered with each other, and the overall wake of the wind turbine widened laterally.

In this study, we investigated the interference between wind turbine wakes and towers in yaw conditions and clarified the mechanism behind the asymmetry of wake formation in yaw wind turbines. The results of this study will aid in developing more accurate wake models and control methods, contributing to the profitable construction and operation of wind farms. However, the large size of the nacelle and tower relative to the rotor diameter of the wind turbine model used in this study strongly affected the results. To further refine the study of yaw wind turbine wakes, the size and shape of the wind turbine, as well as the effects of constantly changing wind conditions in the actual field of operation, should be fully considered.

Credit author statement

Koichiro Shibuya: Conceptualization, Methodology, Validation, Formal analysis, Investigation, Data Curation, Writing - Original Draft, Writing - Review & Editing, Visualization, Project administration. Takanori Uchida: Software, Resources, Supervision, Funding acquisition.

Declaration of competing interest

The authors declare that they have no known competing financial interests or personal relationships that could have appeared to influence the work reported in this paper.

Data availability

Data will be made available on request.

Appendix

A Validation of LES settings

We verified the accuracy of the computational parameters set by LES by testing their validity. To verify the appropriateness of the size of the computational domain, we defined the parameters Lx and Ly, which determine the domain size in the x and y directions, respectively, as illustrated in Fig. A.1. Additionally, we varied the lattice widths Δx and Δy in the x and y directions, respectively, for the regions related to Lx and Ly to assess the impact of lattice width on the results (Fig A.2). The results are presented in Fig. A.3, and it can be observed that the results are consistent across all parameters, indicating that the computational domain is sufficiently large to ensure adequate lattice resolution.

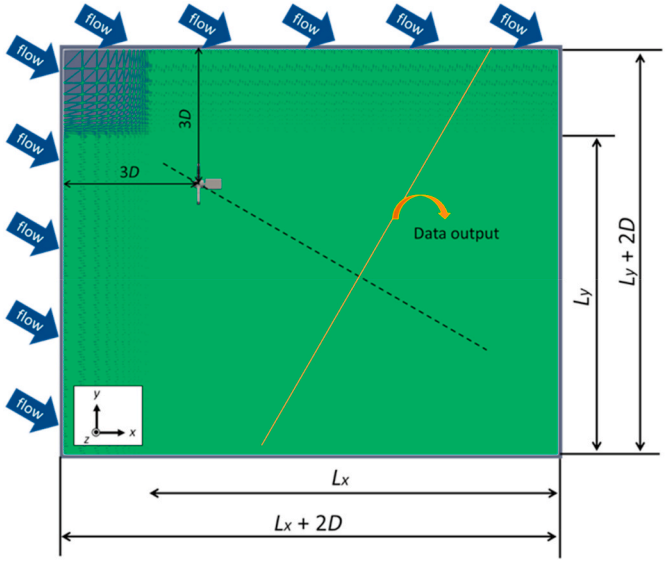

Fig. A.1. Parameter definition of calculation domain sizes.

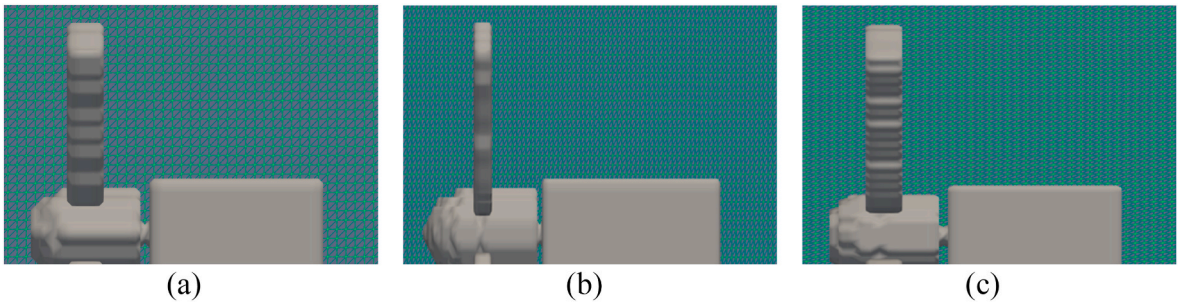

Fig. A.2. Grid width setting: (a) $\Delta x = 0.02D$, $\Delta y = 0.02D$, (b) $\Delta x = 0.01D$, $\Delta y = 0.02D$, (c) $\Delta x = 0.02D$, $\Delta y = 0.01D$.

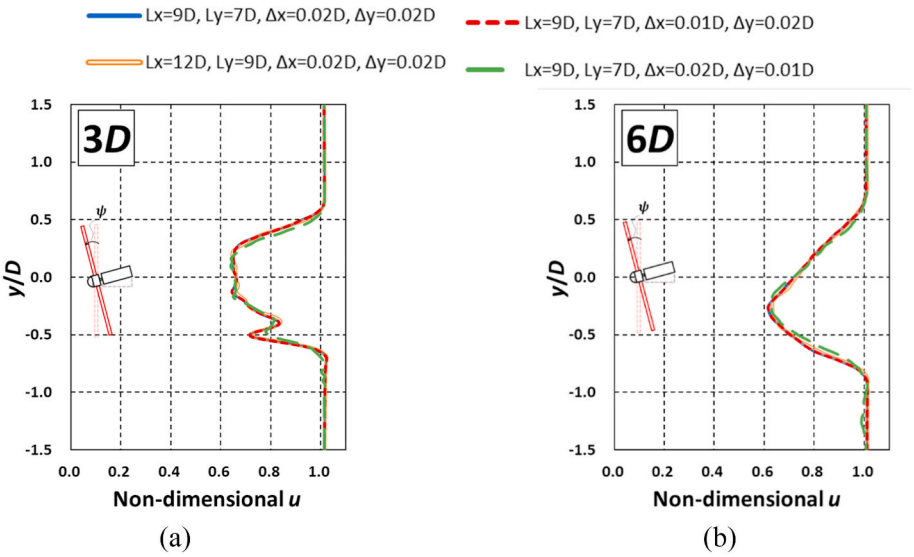

Fig. A.3. Comparison of calculation results for different computational domain sizes and grid widths A parameter study was also conducted to investigate the influence of the dimensionless time interval used for time averaging under the conditions of $Lx = 9D$, $Ly = 7D$, and $\Delta x = \Delta y = 0.02D$. The results, presented in Fig. A.4, demonstrate that data with a dimensionless time of 11 or longer can be used without any issues.

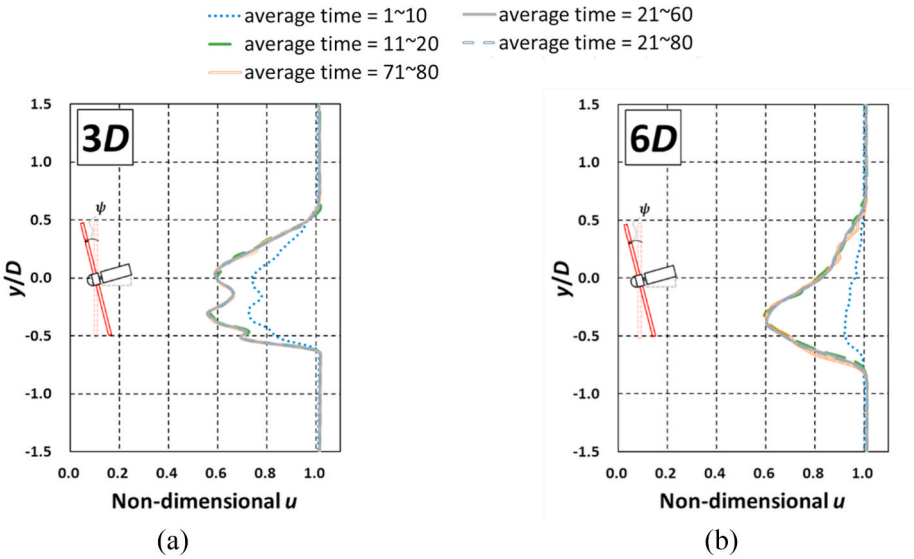

Fig. A.4. Comparison of horizontal distributions by time-averaged interval.

References

[1] Uchida T, Yoshida T, Inui M, Taniyama Y. Doppler lidar investigations of wind turbine near-wakes and LES modeling with new porous disc approach. Energies 2021;14:2101. https://doi.org/10.3390/en14082101.

[2] Thomsen K, Sørensen P. Fatigue loads for wind turbines operating in wakes. J Wind Eng Ind Aerod 1999;80:121–36. https://doi.org/10.1016/S0167-7105(98)00194-9.

[3] Houck DR. Review of wake management techniques for wind turbines. Wind Energy 2021;25:195–220. https://doi.org/10.1002/we.2668.

[4] Meyers J, Bottasso C, Dykes K, Fleming P, Gebraad P, Giebel G, Gocmen T, Van Wingerden JW. Wind farm flow control: prospects and challenges. Wind Energy Sci 2022;7:2271–306. https://doi.org/10.5194/wes-7-2271-2022.
[5] Ciri U, Rotea MA, Leonardi S. Effect on the turbine scale on yaw control. Wind Energy 2018;21:1395–405. https://doi.org/10.1002/we.2262.
[6] Uchida T, Shibuya K, Calderon-Munoz WR, Richmond-Navvaro G. A wind tunnel investigation of yawed wind turbine wake impacts on downwind wind turbine performances and wind loads. Wind Eng 2023:1–16. https://doi.org/10.1177/0309524x221150219.
[7] Bromm M, Rott A, Beck H, Vollmer L, Steinfeld G, Kuhn M. Field investigation on the influence of yaw misalignment on the propagation of wind turbine wakes. Wind Energy 2018;21:1011–28. https://doi.org/10.1002/we.2210.
[8] Archer CL, Vasel-Be-Hagh A. Wake steering via yaw control in multi-turbine wind farms: recommendations based on large-eddy simulation. Sustain Energy Technol Assessments 2019;33:34–43. https://doi.org/10.1016/j.seta.2019.03.002.
[9] Dhiman HS, Deb D, Muresan V, Balas VE. Wake management in wind farms: an adaptive control approach. Energies 2019;12:1247. https://doi.org/10.3390/en12071247.
[10] Fleming PA, Ning A, Gebraad PMO, Dykes K. Wind plant system engineering through optimization of layout and yaw control. Wind Energy 2016;19:329–44. https://doi.org/10.1002/we.1836.
[11] Gebraad PMO, Teeuwisse FW, Pao LY. Wind plant power optimization of layout and yaw control. Wind Energy 2016;19:95–114. https://doi.org/10.1002/we.1822.
[12] Kim C, Gui Y, Chung CC. Maximum power tracking of a wind power plant with predictive gradient ascent method. IEEE Trans Sustain Energy 2017;8:685–94. https://doi.org/10.1109/TSTE.2016.2615315.
[13] Lin M, Porte-Agel F. Power maximization and fatigue-load mitigation in a wind-turbine array by active yaw control: an LES study. J Phys Conf Ser 2020;1618:042036. https://doi.org/10.1088/1742-6596/1618/4/042036.
[14] Qian GW, Ishihara T. Wind farm power maximization thorough wake steering with a new multiple wake model for prediction of turbulence intensity. Energy 2021;220:119680. https://doi.org/10.1016/j.energy.2020.119680.
[15] van Dijk MT, van Wingerden JW, Ashuri T, Li YY. Wind farm multi-objective wake redirection for optimizing power production and loads. Energy 2017;121:561–9. https://doi.org/10.1016/j.energy.2017.01.051.
[16] Yang QS, Li H, Li T, Zhou XH. Wind farm layout optimization for levelized cost of energy minimization with combined analytical wake model and hybrid optimization strategy. Energy Convers Manag 2021;248:114778.
[17] Qian GW, Ishihara T. A new analytical wake model for yawed wind turbines. Energies 2018;11:665. https://doi.org/10.3390/en11030665.
[18] Fleming P, Gebraad PMO, Lee S, van Wingerden JW, Johnson K, Churchfield M, Michalakes J, Spalart P, Moriarty P. Simulation comparison of wake mitigation control strategies for a two-turbine case. Wind Energy 2015;18:2135–43. https://doi.org/10.5194/10.1002/we.1810.
[19] Fleming P, Annoni J, Churchfield M, Martinez-Tossas LA, Gruchalla K, Lawson M, Moriarty P. A simulation study demonstrating the importance of large-scale trailing vortices in wake steering. Wind Energy Sci 2018;3:243–55. https://doi.org/10.5194/wes-3-243-2018.
[20] Miao WP, Li C, Xie XY. Investigation of wake characteristics of a yawed HAWT and its impacts on the inline downstream wind turbine using unsteady CFD. J Wind Eng Ind Aerod 2017;168:60–71. https://doi.org/10.1016/j.jweia.2017.05.002.
[21] Ashton R, Viola F, Camarri S, Gallaire F, Iungo GV. Hub vortex instability within wind turbine wakes: effects of wind turbulence, loading conditions, and blade aerodynamics. Phys Rev Fluids 2016;1:073603. https://doi.org/10.1103/PhysRevFluids.1.073603.
[22] Felli M, Camussi R, Di Felice F. Mechanisms of evolution of the propeller wake in the transition and far fields. J Fluid Mech 2011;682:5–53. https://doi.org/10.1017/jfm.2011.150.
[23] Iungo GV, Viola F, Camarri S, Porte-Agel F, Gallaire F. Linear stability analysis of wind turbine wakes performed on wind tunnel measurements. J Fluid Mech 2013;737:499–526. https://doi.org/10.1017/jfm.2013.569.
[24] Viola F, Iungo GV, Camarri S, Porte-Agel F, Gallaire F. Prediction of the hub vortex instability in a wind turbine wake: stability analysis with eddy-viscosity models cakibrated on wind tunnel data. J Fluid Mech 2014;750:R1. https://doi.org/10.1017/jfm.2014.263.
[25] Pierella F, Saetran L. Wind tunnel investigation on the effect of the turbine tower on wind turbines wake symmetry. Wind Energy 2017;20:1753–69. https://doi.org/10.1002/we2120.
[26] Kono T, Kiwata T. LES analysis of wind turbine tower effects on wake and aerodynamic forces. Proc 23th National Symp on Wind Eng; 2014. p. 139–44 [jstage Publishing].
[27] Abraham A, Dasari T, Hong J. Effect of turbine nacelle and tower on the near wake of utility-scale wind turbine. J Wind Eng Ind Aerod 2019;193:103981. https://doi.org/10.1016/j.jweia.2019.103981.
[28] Matsumiya H, Kogaki T, Takahashi N, Iida M, Waseda K. Development and experimental verification of the new MEL airfoil series for wind turbines. Proc Japan Wind Energy Symp 2011;22:92–5. https://doi.org/10.11333/jweasympo1979.22.92.
[29] Sedaghatizadeh N, Arjomand M, Kelso R, Cazzolato B, Ghayesh MH. Effect of wall confinement on a wind turbine wake. 20th Austral Fluid Mech Conf; 2016. p. 5–8. https://hdl.handle.net/2440/104906.
[30] Kim J, Moin P. Application of a fractional-step method to incompressible Navier-Stokes equations. J Comput Phys 1985;59:308. https://doi.org/10.1016/0021-9991(85)90148-2.
[31] Kajishima T. Upstream-shifted interpolation method for numerical simulation of incompressible flows. Trans J Soc Mech Eng Ser B 1994;60:3319–26. https://doi.org/10.1299/KIKAIB.60.3319.
[32] Kawamura T, Takami H, Kuwahara K. Computation of high Reynolds number flow around a circular cylinder with surface roughness. Fluid Dynam Res 1986;1:145–62. https://doi.org/10.1016/0169-5983(86)90014-6.
[33] Inagaki M, Kondoh T, Nagano Y. A mixed-time-scale SGS model with fixed model-parameters for practical LES. ASME J Fluids Eng 2005;127:1–13. https://doi.org/10.1115/1.1852479.
[34] Uchida T, Li G. Comparison of RANS and LES in the prediction of airflow field over steep complex terrain. Open J Fluid Dynam 2018;8:286–307. https://doi.org/10.4236/ojfd.2018.83018.
[35] Sørensen JN, Shen WZ. Numerical modeling of wind turbine wakes. J Fluid Eng 2002;124:393–9. https://doi.org/10.1115/1.1471361.
[36] Krogstad PA, Adaramola MS. Performance and near wake measurements of a model horizontal axis wind turbine. Wind Energy 2012;15:743–56. https://doi.org/10.1002/we.502.